Targeting methionine synthase in a fungal pathogen causes a metabolic imbalance that impacts cell energetics, growth and virulence

Jennifer Scott[1], Monica Sueiro-Olivares[1], Benjamin P. Thornton[2], Rebecca A. Owens[3], Howbeer Muhamadali[4], Rachael Fortune-Grant[1], Riba Thomas[1], Katherine Hollywood[5], Sean Doyle[3], Royston Goodacre[4], Lydia Tabernero[2], Elaine Bignell[1] and Jorge Amich[1]*

1. Manchester Fungal Infection Group (MFIG), Division of Infection, Immunity and Respiratory Medicine, School of Biological Sciences, Faculty of Biology, Medicine and Health, University of Manchester, Manchester Academic Health Science Centre, Manchester, UK.
2. School of Biological Sciences, Faculty of Biology, Medicine and Health, University of Manchester, Manchester Academic Health Science Centre, Manchester, UK.
3. Department of Biology, Maynooth University, Co. Kildare, Ireland.
4. Department of Biochemistry, Institute of Integrative Biology, University of Liverpool, Liverpool, UK.
5. Manchester Institute of Biotechnology. University of Manchester, Manchester, UK.

*Corresponding author: jorge.amichelias@manchester.ac.uk

ABSTRACT

There is an urgent need to develop novel antifungals to tackle the threat fungal pathogens pose to human health. In this work, we have performed a comprehensive characterisation and validation of the promising target methionine synthase (MetH). We uncover that in *Aspergillus fumigatus* the absence of this enzymatic activity triggers a metabolic imbalance that causes a reduction in intracellular ATP, which prevents fungal growth even in the presence of methionine. Interestingly, growth can be recovered in the presence of certain metabolites, which evidences that *metH* is a conditionally essential gene. As this implies that for a correct validation MetH should be targeted in established infections, we have optimised a genetic model to mimic treatment of established infections using the tetOFF system. We show that repression of *metH* in growing hyphae halts growth *in vitro*, which translates into a beneficial effect when targeting established infections using this model *in vivo*. Finally, a structural-based virtual screening of methionine synthases reveals key differences between the human and fungal structures and unravels features in the fungal enzyme that can guide the design of novel specific inhibitors. Therefore, methionine synthase is a valuable target for the development of new antifungals.

AUTHOR SUMMARY

Fungal pathogens are responsible for millions of life-threatening infections on an annual basis worldwide. The current repertoire of antifungal drugs is very limited and, worryingly, resistance has emerged and already become a serious threat to our capacity to treat fungal diseases. The first step to develop new drugs often is to identify molecular targets which inhibition during infection can prevent pathogen growth. However, the current models are not suitable to validate targets in established infections. Here we have characterised the promising antifungal target methionine synthase in great detail, using the prominent fungal pathogen *Aspergillus fumigatus* as a model. We have uncovered the underlying reason for its essentiality and confirmed its druggability. Furthermore, we have optimised the use of a genetic system to show a beneficial effect of targeting methionine synthase in established infections. Therefore, we believe that antifungal drugs to target methionine synthase should be pursued and additionally, we propose that antifungal targets should be validated in a model of established infection.

61 **INTRODUCTION**

62 Fungal pathogens represent an increasing risk to human health (1), with over one billion people
63 worldwide affected by mycoses annually. Many of these mycoses are superficial infections of
64 the skin, nails or mucosal membranes and although troublesome are usually not life-
65 threatening. However, some fungi cause devastating chronic and invasive fungal infections,
66 which result in an estimated 1.6 million deaths per year (2). Incidences of invasive infections
67 caused by *Aspergillus*, *Candida*, *Cryptococcus* and *Pneumocystis* species are increasing (3), a
68 cause for serious concern as these genera are responsible for 90% of deaths caused by mycoses
69 (4). Despite the availability of antifungal drugs, mortality rates for invasive aspergillosis, invasive
70 candidiasis, cryptococcal meningitis and *Pneumocystis jirovecii* pneumonia are intolerably high,
71 reaching over 80%, 40%, 50% and 30% respectively (2, 5). There are currently only four classes
72 of antifungals in clinical use to treat invasive infections (azoles, echinocandins, polyenes and
73 flucytosine), all suffering from pharmacological drawbacks including toxicity, drug-drug
74 interactions and poor bioavailability (6, 7). With the sole exemption of flucytosine, which is only
75 used in combinatory therapy with amphotericin B for cryptococcal meningitis and *Candida*
76 endocarditis (7), the current antifungals target critical components of the fungal cell membrane
77 or cell wall (8), which represents a very limited druggable space. The rise of antifungal resistance
78 presents an additional challenge as mortality rates in patients with resistant isolates can reach
79 100%, making the development of new antifungal drugs increasingly critical for human health
80 (1, 9). Targeting fungal primary metabolism is broadly considered a valid strategy for the
81 development of novel antifungals, as it is crucial for pathogen virulence and survival (10, 11). A
82 primary example of success of this strategy is olorofim (F901318), a novel class of antifungal that
83 targets the pyrimidine biosynthesis pathway (12), which is currently in clinical trials.

84 Methionine synthases catalyse the transfer of a methyl group from *N*5-methyl-5,6,7,8-
85 tetrahydrofolate (CH_3-THF) to L-homocysteine (Hcy). Two unrelated protein families catalyse
86 this reaction: cobalamin dependent methionine synthases (EC 2.1.1.13) and cobalamin
87 independent methionine synthases (EC 2.1.1.14). Members of both families must catalyse the
88 transfer of a low active methyl group from the tertiary amine, CH_3-THF, to a relatively weak
89 nucleophile, Hcy sulfur. Cobalamin dependent enzymes facilitate this transfer by using
90 cobalamin as an intermediate methyl carrier (13). By contrast, cobalamin independent enzymes
91 directly transfer the methyl group from CH_3-THF to Hcy (14). Logically, proteins of each family
92 differ significantly both at amino acid sequence (15) and 3D structure level (16).

93 We have previously shown that the methionine synthase-encoding gene is essential for *A.*
94 *fumigatus* viability and virulence, which led us to propose it as a promising target for antifungal

95 drug development (17). In support of this, a systematic metabolic network analysis by Kaltdorf
96 and colleagues identified methionine synthase as a promising antifungal drug target worthy of
97 investigation (11). Methionine synthase has also been described as essential for *Candida*
98 *albicans* viability (18, 19) and necessary for *Cryptococcus neoformans* pathogenicity (20), which
99 suggests that a drug developed against this enzyme may have a broad spectrum of action.
100 Moreover, fungal methionine synthases are cobalamin independent, differing significantly from
101 the cobalamin dependent human protein at the amino acid sequence level: only 11.2% identity,
102 20.4% similarity and 60.2% gaps when aligned the *A. fumigatus* and human proteins using L-
103 Align from EMBL (21, 22). Therefore, it should be possible to develop drugs with low toxicity
104 potential.

105 Target validation is critical and has been suggested as the most important step in translating
106 a new potential target into a viable drug target because of its role in achieving efficacy in patients
107 (23). Indeed a retrospective analysis from AstraZeneca's drug pipeline showed that projects that
108 had performed a more thorough target validation were less likely to fail: 73% of the projects
109 were active or successful in Phase II compared with only 43% of projects without such extra
110 target validation (24). Therefore, in this work we aimed to further substantiate methionine
111 synthase's potential as an antifungal drug target, before advancing the drug discovery process.
112 In particular, we were interested in 1) unravelling the mechanistic basis of methionine synthase
113 essentiality in *A. fumigatus*, which is needed to fully explore the potential of this enzyme as drug
114 target and to be able to anticipate drug resistance mechanisms; and 2) developing *in vivo* models
115 of infection to mimic treatment against the target in an established infection and using them to
116 validate methionine synthase as an antifungal drug target.

117

118 **RESULTS AND DISCUSSION**

119 *Methionine synthase enzymatic activity is essential for Aspergillus fumigatus viability*

120 We had previously demonstrated that the methionine synthase encoding gene is essential for
121 *A. fumigatus* viability and virulence (17); however, the underlying reason for this essentiality was
122 still unclear. To address this question, here we have constructed strains that express the *metH*
123 gene under the control of a tetOFF system recently adapted for *Aspergillus* (25) in two different
124 *A. fumigatus* wild-type backgrounds, ATCC46645 and A1160. The advantage of the tetOFF
125 system over other regulatable systems is that doxycycline (Dox) can be added to downregulate
126 gene expression in growing hyphae (Fig. S1A), and thus this system permits investigation of the
127 consequences of the repression of an essential gene in growing mycelia. The constructed

128 *metH_tetOFF* strains (*H_OFF*) grew as the wild type in the absence of Dox, but as little as 0.5
129 µg/mL was sufficient to completely prevent colony development on an agar plate even in the
130 presence of methionine (Fig. S1B). This corroborates our previous result that methionine
131 synthase is essential for *A. fumigatus* viability and that its absence does not result in a sheer
132 auxotrophy for methionine (17).

133 Methionine synthase forms an interjection between the trans-sulfuration pathway and the
134 one carbon metabolic route (Fig. 1A), as the enzyme utilizes 5-methyl-tetrahydrofolate as co-
135 substrate. Therefore, the essentiality of *metH* might be due to required integrities of the trans-
136 sulfuration pathway or of the one carbon metabolic route. Alternatively, it could be that the
137 presence of the enzyme itself is essential, either because its enzymatic activity is required or
138 because it is fulfilling an unrelated additional role, as being part of a multiprotein complex. To
139 start discerning among these possibilities, we constructed a double *ΔmetGΔcysD* mutant,
140 blocked in the previous step of the trans-sulfuration pathway, and a *ΔmetF* deletant, which
141 blocks the previous step of the one-carbon metabolic route (Fig. 1A). As we had previously
142 observed (26), to rescue fully *ΔmetF*'s growth the media had to be supplemented with
143 methionine and other amino acids, as the folate cycle is necessary for the interconversion of
144 serine and glycine and plays a role in histidine and aromatic amino acid metabolism (27, 28).
145 Consequently, we added a mix of all amino acids except cysteine and methionine to the S-free
146 medium for this experiment. Phenotypic tests (Fig. 1B) confirmed that the *ΔmetGΔcysD* and
147 *ΔmetF* mutants were viable and could grow in the presence of methionine. In contrast, the
148 *H_OFF* conditional strain could not grow under restrictive conditions even in the presence of the
149 amino acid mix and methionine (Fig. 1B). Therefore, the MetH protein itself, and not the integrity
150 of the trans-sulfuration and one-carbon pathways, is essential for *A. fumigatus* viability.
151 Interestingly, the methionine auxotroph *ΔmetGΔcysD* was avirulent in a leukopenic model of
152 pulmonary aspergillosis (Fig. S1C), suggesting that the amount of readily available methionine
153 in the lung is very limited, not sufficient to rescue its auxotrophy. Indeed, the level of methionine
154 in human serum was calculated to be as low as ~20 µM (29, 30), which was described as
155 insufficient to support the growth of various auxotrophic bacterial pathogens (31) and we have
156 also observed that is not enough to rescue growth of the *A. fumigatus ΔmetGΔcysD* auxotroph.

157 Essentiality of the MetH protein could be directly linked to its enzymatic activity or,
158 alternatively, the protein could be performing an additional independent function. To discern
159 between these two possibilities, we constructed two strains that express single-point mutated
160 versions of MetH from the innocuous Ku70 locus of the *H_OFF* background strain, under the
161 control of its native promoter (Fig. 1C). These point mutations, $metH^{g2042A>2C}$ (D616A) and

162 *metH*$^{g2179TA>9GC}$ (Y662A), were previously described to prevent conformational rearrangements
163 required for activity of the *C. albicans* methionine synthase (32). In the absence of Dox, these
164 strains grew normally, as they expressed both the wild-type MetH, from the tetOFF promoter,
165 and the mutated version of the protein (Fig. 1C). In the presence of Dox, when the wild-type
166 *metH* gene was downregulated, the Y662A strain grew on sulfate worse than in non-restrictive
167 conditions, but still to a significant extent, suggesting that this point mutation did not completely
168 abrogate enzymatic activity (Fig. 1C). Interestingly, Y662 grew normally on methionine, showing
169 that methionine can compensate for a partial reduction of MetH activity (Fig 1C). The D616A
170 strain (two isolates were tested) was not able to grow on sulfate (Fig. 1C), demonstrating that
171 enzymatic activity was fully blocked. Nor could it grow on methionine (Fig. 1C), indicating that
172 enzymatic activity is required for viability even in the presence of the full protein. The D616A
173 version of the protein was confirmed to be stable as a GFP-tagged protein could be visualised in
174 -Dox conditions (not shown). All these phenotypes support the conclusion that methionine
175 synthase enzymatic activity is required for viability.

176

177 *Absence of methionine synthase enzymatic activity results in a shortage of crucial metabolites,*
178 *but does not cause toxic accumulation of homocysteine*

179 The absence of methionine synthase enzymatic activity has two direct consequences, which
180 could cause deleterious effects and therefore explain its essentiality (Fig. 1A). It could cause an
181 accumulation of the potentially toxic substrate homocysteine and a shortage of the co-product
182 tetrahydrofolate (THF). THF is directly converted to 5,10-methylene-THF, which is required for
183 the synthesis of purines and thymidylate (TMP), and thus for DNA synthesis; additionally, as
184 purine biosynthesis requires Gln, Gly and Asp, and THF *de novo* synthesis requires chorismate
185 (precursor of aromatic amino acids), a shortage of THF might cause a depletion of amino acids
186 (Fig. 1A). To investigate if the depletion of any of these metabolites underlies MetH essentiality,
187 we supplemented the media with a number of precursors and potentially depleted metabolites
188 (Fig. 2A). Added as sole supplement, only adenine was able to trigger growth, but to a minimal
189 degree. Further addition of a mixture of all amino acids noticeably improved growth.
190 Supplementation with adenine and guanine (purine bases) did also reconstitute noticeable
191 growth, which was not enhanced with further addition of amino acids. Folic acid was also
192 capable of reconstituting growth, but only when amino acids were added as the sole N-source
193 (Fig. S3). However, no combination of compounds was able to reconstitute growth to the wild-
194 type level. This suggests that a shortage of relevant metabolites derived from THF, prominently
195 adenine, partially accounts for methionine synthase essentiality, but cannot explain it

196 completely. In other fungi, as *Pichia pastoris* (33) or *Schizosaccharomyces pombe* (34),
197 summplementation with methionine and adenine was found to restore growth of a *metH*
198 mutant to wild-type levels, denoting them as combined auxotrophs. In *A. fumigatus* it seems to
199 be more complex because supplementation with methionine, adenine and other amino acids
200 did not restore growth fully, suggesting that more factors are implicated.

201 To investigate if homocysteine could be accumulating to toxic levels in the absence of MetH
202 activity, we over-expressed several genes that should alleviate its accumulation. To this aim we
203 designed and constructed the plasmid pJA49, which allows direct integration of any ORF to
204 episomally overexpress genes in *A. fumigatus*. Plasmid pJA49 carries the *A. nidulans* AMA1
205 autologous replicating sequence (35, 36) and the hygromycin B resistance gene (*hygrB*) as a
206 selection marker. A unique *Stu*I restriction site allows introduction of any PCR amplified ORF in
207 frame under the control of the *A. fumigatus* strong promoter *hspA* (37) and the *A. nidulans trpC*
208 terminator (Fig S2A). Using this plasmid, we produced a strain in the *H_OFF* background that
209 episomally overexpresses *mecA,* encoding cystathionine-β-synthase, which converts
210 homocysteine to cystathionine (Fig. 1A). Homocysteine exerts toxic effects through its
211 conversion to *S*-adenosylhomocysteine, which causes DNA hypomethylation (38, 39), or to
212 homocysteine thiolactone, which causes *N*-homocysteinylation at the ε-amino group of protein
213 lysine residues (40, 41). Consequently, we also constructed strains that episomally over-express
214 genes that could detoxify those products: the *S*-adenosyl-homocysteinase lyase encoding gene
215 *sahL* (AFUA_1G10130) or the *A. nidulans* homocysteine thiolactone hydrolase encoding gene
216 *blhA* (AN6399) (*A. fumigatus* genome does not encode any orthologue) (Fig. S2B). However,
217 despite a strong over-expression of the genes (Fig. S2C&D), none of them could rescue growth
218 of the *H_OFF* strain in restrictive conditions (Fig. 2B). Therefore, our over-expression
219 experiments suggest that homocysteine accumulation is not responsible for *metH* essentiality,
220 but additional experiments such as quantification homocysteine levels, which are currently
221 challenging, would be required to further support this hypothesis. Addition of adenine to the
222 medium did not improve growth of the overexpression strains further than that of the *H_OFF*
223 background (Fig. 2B), indicating that there is likely not a combined effect of homocysteine
224 accumulation and depletion of THF-derived metabolites. Toxic accumulation of homocysteine
225 was speculated to be the underlying reason of methionine synthase essentiality in both *Candida*
226 *albicans* and *Cryptococcus neoformans* (19, 20) but our results suggest that this is not the case
227 in *A. fumigatus*. Therefore, we propose that the previous assumption should be revisited in
228 other fungal pathogens.

229

230 *Methionine synthase repression triggers a metabolic imbalance that causes a decrease in cell*
231 *energetics*

232 Aiming to identify any adverse metabolic shift in the absence of MetH and/or accumulation of
233 toxic compounds that could explain its necessity for proper growth, we performed a
234 metabolomics analysis, via gas chromatography-mass spectrometry (GC-MS), comparing the
235 metabolites present in wild-type and *H_OFF* strains before and after Dox addition. Before Dox
236 addition both strains clustered closely together in a Principal Component Analysis (PCA) scores
237 plot (Fig. S4A), showing that their metabolic profiles are highly similar. However, 6 h after Dox
238 addition the strains clusters became clearly separated, denoting differential metabolite content.
239 Analysis of the differentially accumulated metabolites (full list can be consulted in Table S1)
240 using the online platforms MBRole (42) and Metaboanalyst (43, 44) did not reveal any obvious
241 metabolic switch, probably due to the rather small number of metabolites that could be
242 identified by cross-referencing with the Golm library (http://gmd.mpimp-golm.mpg.de/).
243 Manual inspection of the metabolites pointed out interesting aspects. Firstly, the methionine
244 levels were not significantly different, which demonstrates that methionine supplementation in
245 the growth medium triggers correct intracellular levels in the *H_OFF* strain; this undoubtedly
246 rules out that a shortage of methionine could be the cause of the essentiality of methionine
247 synthase. Secondly, we detected a significantly lower amount of adenosine in the *H_OFF* strain
248 compared with the wild-type after Dox addition (Fig. 3A), which is in agreement with our
249 previous result that supplementation of adenine can partially reconstitute growth in the
250 absence of MetH. We did not find accumulation of compounds with a clear toxic potential upon
251 *metH* repression. Nevertheless, we detected a lower amount of several amino acids (Phe, Ser,
252 Glu, Pro, Ile, Thr, Ala and Asp, Fig. S4B), which suggests that the cells may enter into growth
253 arrest upon *metH* repression. Interestingly, we noticed a significantly lower accumulation of
254 some metabolites of the glycolysis pathway and TCA cycle (Fig. 3A) and some other mono and
255 poly-saccharides (Fig. S4B). These variations could reflect a low energetic status of the cells upon
256 *metH* repression. Indeed, we found that the level of ATP significantly decreased in the *H_OFF*
257 strain upon Dox addition (Fig. 3B). Therefore, we evaluated if supplementation of the medium
258 with substrates that have the potential to increase cell energetics can rescue *H_OFF* growth in
259 restrictive conditions. We found that when pyruvate, which can directly be converted to acetyl-
260 CoA to enter the TCA cycle, was added as the sole carbon source *H_OFF* growth was
261 reconstituted in restrictive conditions to the same level as the wild-type (Fig. 3C). Growth was
262 limited for both strains, as pyruvate does not appear to be a good carbon source (45). However,
263 the presence of glucose in the medium precluded the reconstitution of growth of *H_OFF* (Fig.

264 S3), as it has been described to prevent pyruvate uptake in *S. cerevisiae* (46). We next tested the
265 capacity of ATP to be used an alternative energy source and to reconstitute growth. To diversify
266 the presence of permeases in the cell membrane, and thus maximise the chance of ATP uptake,
267 we assayed two different N-sources: ammonium (NH_4^+, preferred source) and amino acids (Fig.
268 S3). Indeed, when amino acids were the only N-source, supplementation of the medium with
269 ATP reconstituted *H_OFF* growth in restrictive conditions to wild type levels (Fig. 3C). This agrees
270 with the recent observation that eukaryotic cells can uptake ATP and exploit it as an energy
271 source (47). In conclusion, a decrease in cell energetics developed in the absence of methionine
272 synthase seems to be able to explain MetH essentiality for growth.

273 The fact that growth in the absence of methionine synthase can be reconstituted when there
274 are sufficient levels of ATP implies that *metH* is a conditionally essential gene, meaning that it is
275 only essential in the absence of the specific conditions that overcome the disturbances derived
276 from its deficiency. We believe that a significant number of genes previously described as
277 essential in fungi would in fact be conditionally essential, however the right conditions to
278 reconstitute growth have not been identified in many cases. This highlights a paramount
279 consideration for the proper identification and validation of drug targets: the deficiencies
280 introduced by targeting a conditionally essential gene must not be overcome during infection.
281 This important concept has already been discussed by others (48-51) and we believe addressing
282 it should become the standard for antimicrobial target validation. In the case of methionine
283 synthase, it is unlikely that the fungus could acquire sufficient levels of ATP (combined with
284 methionine and not using preferred N-source) in the lung tissue to overcome the growth defect
285 resulting from targeting MetH. The concentration of free extracellular ATP in human plasma has
286 been calculated to be in the sub-micromolar range (28-64 nM) (52). In the lungs, extracellular
287 ATP concentrations must be strictly balanced and increased levels are implicated in the
288 pathophysiology of inflammatory diseases (53); nevertheless, even in such cases ATP levels have
289 been calculated in the low micromolar range (54, 55). In any case, MetH needs to be validated
290 in a suitable model to corroborate that its deficiency cannot be not overcome in established
291 infections.

292 We then questioned how the lack of methionine synthase's enzymatic activity could cause a
293 drop in cell energy. We hypothesised that blockage of methionine synthase activity likely causes
294 a forced conversion of 5,10-methylene-THF to 5-methyl-THF by the action of MetF (Fig. 1A). In
295 support of this, we observed that expression of *metF* was increased in the *H_OFF* strain (Fig. 3D).
296 This likely causes a shortage of 5,10-methylene-THF, as the conversion is not reversible and THF
297 cannot be recycled by the action of methionine synthase (Fig. 1A). Indeed, supplementation of

298 folic acid (only when amino acids are the sole N-source, Fig. S3) and of purines could partially
299 restore growth (Fig. 2A), as they compensate for the deficit in purine ring biosynthesis when
300 there is a shortage of 5,10-methylene-THF. However, this still does not explain why there is a
301 drop in ATP. We hypothesised that the block of purine biosynthesis might be sensed as a
302 shortage of nucleotides. This could then cause a shift in glucose metabolism from glycolysis and
303 the TCA cycle (which produce energy) to the Pentose Phosphate Pathway (PPP), which is
304 required to produce ribose-5-phosphate, an integral part of nucleotides. In a similar vein, it has
305 recently been described that activation of anabolism in *Saccharomyces cerevisiae* implies
306 increased nucleotide biosynthesis and consequently metabolic flow through the PPP (56). To
307 evaluate our hypothesis, we investigated the transcription level of the glucose-6-phosphate
308 dehydrogenase (G6PD) encoding gene (AFUA_3G08470), which catalyses the first committed
309 step of the PPP. In agreement with our hypothesis, the expression of G6PD encoding gene
310 increases in the *H_OFF* strain upon addition of Dox (Fig. 3D), likely reflecting an increased flow
311 through the PPP. We then wondered how cells may be activating the PPP. The target of
312 rapamycin (TOR) TORC1 effector, which is widely known to activate anabolism and growth (57-
313 59), has been described to activate the PPP in mammalian cells (60, 61) and has been
314 functionally connected with energy production and nucleotide metabolism in *A. fumigatus* (62).
315 In addition, the cAMP/PKA (protein kinase A) pathway is known to be paramount for sensing of
316 nutrients and the correspondent adaptation of gene expression and metabolism (63), and was
317 found to be implicated in the regulation of nucleotide biosynthesis in *A. fumigatus* (64).
318 Consequently, we explored if a partial block of TOR with low concentrations of rapamycin or of
319 PKA with H-89 could prevent the imbalanced activation of the PPP in the absence of MetH
320 activity. However, neither of the inhibitors could reconstitute growth of the *H_OFF* strain in
321 restrictive conditions (Fig. S4C). This means that neither the TOR nor the PKA pathways seem to
322 be involved in the deleterious metabolic shift that seemingly activates PPP and decreases flux
323 through glycolysis. Therefore, more experiments are required to confirm our hypothesis and
324 elucidate the mechanism.

325 In summary, we propose that absence of methionine synthase activity causes a strong defect
326 in purine biosynthesis that the cell tries to compensate for by shifting carbon metabolism to the
327 PPP; this metabolic imbalance causes a drop of ATP levels, which collapses cell energetics and
328 results in halted growth (Fig. 3E).

329 Interestingly, we also detected that *metF* expression is higher in the *H_OFF* strain compared
330 to the wild-type, even in the absence of Dox (Fig. 3D). This could be explained as an effort to
331 compensate a higher demand of 5-methyl-THF by the slightly increased amount of methionine

332 synthase in this strain (Fig. S1A). This effect could cause a mild defect in purine biosynthesis in
333 the *H_OFF* strain, and indeed adenosine content was lower in the *H_OFF*–Dox condition
334 compared with the wild-type–Dox sample in the metabolome analysis (Fig 3A). Furthermore,
335 this also explains why we detected a small but significant increase of G6PD expression in the
336 *H_OFF*-Dox condition (Fig. 3D). Therefore, it seems that upregulating methionine synthase has
337 the potential to cause the same metabolic imbalance as downregulating it. However, the effect
338 of overexpression (notice that it is only ~1.5 fold in our strain Fig. S1A) is minor and does not
339 have obvious consequences for growth, as THF can be recycled and thus the shortage of 5,10-
340 methylene-THF is not severe. In any case, two important points can be highlighted from this
341 small imbalance. Firstly, methionine synthase activity is very important and must be finely tuned
342 to maintain a proper metabolic homeostasis. Secondly, changing the expression level of genes
343 with constitutive and/or regulatable promoters can have unexpected and hidden consequences
344 that often go unnoticed.

345

346 *Supplementation with S-adenosylmethionine reconstitutes ATP levels and growth*

347 We have shown that the absence of MetH activity causes a reduction in ATP levels. *S*-
348 adenosylmethionine (SAM) is produced from methionine and ATP by the action of *S*-
349 adenosylmethionine synthetase SasA (Fig. 1A), an essential enzyme in *A. nidulans* (65). Hence,
350 we reasoned that the absence of MetH activity might cause a decrease in SAM levels. To test
351 that hypothesis, we first attempted to rescue growth of the *H_OFF* strain in a medium
352 supplemented with methionine and SAM. We tested various N-sources to diversify the presence
353 of permeases in the cell membrane, aiming to maximise the chances of SAM uptake (Fig. S3).
354 Indeed, the addition of SAM reconstituted growth of the *H_OFF* strain in restrictive conditions
355 in the presence of methionine when amino acids were the only N-source (Fig. 4A and S3). We
356 then measured the intracellular concentration of SAM in growing mycelia upon addition of Dox
357 using MS/MS. Surprisingly, we observed that addition of Dox to the *H_OFF* strain did not cause
358 a significant reduction in SAM levels (Fig. 4B). Consequently, we wondered how the addition of
359 SAM may reconstitute *H_OFF* growth if its levels are not reduced upon *metH* repression. We
360 speculated that as SAM is a crucial molecule it continues to be produced even if the levels of
361 ATP are reduced, draining it from other cellular processes and thus triggering energy
362 deprivation. In support of this hypothesis, we observed that supplementing SAM to the medium
363 increased the levels of ATP in growing hyphae (Fig. 4C).

364 As SAM supplementation can reconstitute *H_OFF* growth, it constitutes another condition
365 that overcomes the conditional essentiality of *metH*, highlighting again the need to validate
366 MetH in a model of established infection. The concentration of SAM in human serum is
367 extremely low, in the range of 100-150 nM (30), and consequently it is unlikely that the fungus
368 could find sufficient SAM during infection to compensate for the defect in ATP caused by
369 targeting methionine synthase.

370 *S*-adenosylmethionine plays a fundamental role as methyl donor for the majority of cellular
371 methylation reactions, including methylation of DNA. Given the observed importance of SAM in
372 the absence of MetH activity and considering that in *P. pastoris* and *C. albicans* methionine
373 synthase was reported to localise in the nucleus, as well as in the cytoplasm (33), we speculated
374 that nuclear localization might be important for MetH cellular function. To test this hypothesis,
375 we constructed strains expressing different versions of C-terminus GFP-tagged MetH from the
376 pJA49 plasmid (Fig. S2) in the *H_OFF* background. These were a wild-type MetH, a $MetH^{D616A}$
377 (control of no growth –Fig. 1C & S5A–) and a $MetH^{R749A}$ (*metH*$^{g2439CG>GA}$) version of the protein,
378 which according to the results published for *P. pastoris* should not localise in the nucleus (33).
379 The strain expressing wild-type MetH grew normally in restrictive conditions (Fig. S5A), proving
380 that the tagged MetH-GFP protein was active. We confirmed that *A. fumigatus* MetH localises
381 in both the nucleus and cytoplasm (Fig 4D & S5B). In contrast to what was described in *P.*
382 *pastoris*, the $MetH^{R749A}$ protein seems to be active, as it could trigger growth of *H_OFF* in
383 restrictive conditions (Fig. S5A) and still localised into the nucleus (Fig. S5B). Therefore, the
384 possibility that MetH localisation in the nucleus is important needs further exploration.

385

386 *Repression of methionine synthase causes growth inhibition in growing mycelia*

387 The major advantage of the tetOFF system is that it can be employed to simulate a drug
388 treatment before a specific chemical is developed. Addition of Dox to a growing mycelium
389 downregulates the gene of interest (Fig S1A), mimicking the effect of blocking its product by the
390 action of a drug. To investigate the effect that blocking MetH has for mycelial growth, we added
391 Dox to 12, 16 or 24 h grown submerged mycelia and left it incubating for an additional 24 h.
392 Addition of Dox to 12 or 16 h grown mycelia severely impaired growth, as observed by biomass
393 (Fig. 5A) and OD (Fig S6A) measurements. This effect was lost when Dox was added to 24 h
394 grown mycelia, due to the incapacity of Dox to reach and downregulate expression in all cells
395 within the dense mass of an overgrown mycelium. Interestingly, Dox addition to methionine free
396 media stopped *H_OFF* growth immediately, which can be observed by comparing fungal biomass

397 at the time of Dox addition to the measurement 24 h after Dox addition. In contrast, the fungus
398 inoculated in methionine containing media grew a little further after Dox addition (Fig. 5A). To
399 understand this difference, we added Dox to either resting or 8 h germinated conidia and imaged
400 them 16 and 40 h after drug addition (Fig. 5B & Fig. S6B). In agreement with the previous result,
401 we observed that Dox addition in methionine free medium inhibited growth immediately:
402 resting conidia did not germinate and germinated conidia did not elongate the germtube. In
403 contrast, after addition of Dox in methionine containing medium, most of the resting conidia
404 were still able to germinate and some germlings could elongate the germinated tubes to form
405 short hyphae. This suggests that the drop in ATP levels takes ~3-4 h before having an effect on
406 growth. Importantly, once growth was inhibited, the effect was sustained for a long period, as
407 we could not detect further growth up to 40 h post-inoculation. To corroborate these
408 observations and further determine whether the effect of growth is fungistatic or fungicidal in
409 the long term, we performed a time-lapse analysis of the effects of adding Dox to 8 h swollen
410 conidia and its subsequent withdrawal after 16 h of incubation (Fig. 5C and Video 1). We
411 observed that growth was inhibited ~4 h after Dox addition and almost completely halted after
412 6 h, which was sustained as long as the drug was present. Upon withdrawal of Dox, growth
413 resumes within 6 h (Fig 5D), showing that the effect of blocking MetH is fungistatic, at least with
414 the genetic TeOFF model of *metH* repression.

415

416 *Targeting MetH in established infections interferes with the progression of disease*

417 Using the TetON system we previously showed that impeding genetic expression of *metH* in the
418 infecting conidia resulted in avirulence in a murine model of invasive pulmonary aspergillosis
419 (17). This demonstrated that the murine lung does not readily provide the conditions to
420 overcome the conditional essentiality of *metH*, and thus this gene is required to establish
421 infection. However, antifungal drugs are normally administered to treat patients who already
422 have an established infection. This could imply that the conditional essentiality of the gene is
423 overcome as the fungal metabolic requirements and the environmental conditions are different
424 when the fungus is actively growing in the tissue (49, 50). Consequently, in order to achieve a
425 rigorous target validation, it is crucial to assess the efficiency of new target candidates in
426 established infections. The first conditional promoter system used for *A. fumigatus in vivo* was
427 the (p)niiA (48). This system represses genetic expression of the gene of interest in the presence
428 of ammonium, which is contained in murine serum. Accordingly, in this seminal study several
429 genes essential *in vitro* were confirmed or refuted to be essential to establish infection in a
430 model of systemic (blood) infection. Currently, two more systems are in use to assess the

431 relevance of fungal essential genes for pulmonary infection: TetON and (p)xylP. These systems
432 can be used to either impede or permit fungal gene expression in murine lungs; but in both
433 models this control must be exerted from the beginning of infection, as sufficient levels of the
434 inducing molecule (doxycycline or xylose) must be present to activate gene expression in the
435 control condition. Consequently, these models have been used to investigate the role of genes
436 that are required to grow *in vitro* to establish pulmonary infection (17, 66, 67). However, those
437 models cannot be used to mimic drug treatments of already established aspergillosis infections
438 *in vivo*. Therefore, we aimed to optimise the use of the TetOFF system for this purpose, as it can
439 be used to downregulate gene expression in growing mycelia. As a control for the model, we
440 constructed a *cyp51A_tetOFFΔcyp51B* (*51A_OFF*) strain. We reasoned that the target of the
441 azoles, first-line treatment drugs for *Aspergillus* diseases, should be the gold standard to
442 compare to for any target. This strain showed a similar behaviour as *H_OFF in vitro*: as little as
443 0.05 µg/ml Dox prevented colony development on an agar plate (Fig. S7A) and addition of Dox
444 to conidia or germlings blocked growth (Fig. S7B).

445 We first assayed the use of the TetOFF system in the *Galleria mellonella* alternative mini-host
446 model of infection. Preliminary experiments revealed that the balance between reaching
447 sufficient levels of Dox to exert an effect and preventing toxic effects of overdose was very
448 delicate. We finally optimised a regimen consisting of 5 injections of 50 mg/kg Dox (Fig. S8A).
449 We then infected *Galleria* larvae with 5×10^2 conidia of *51A_OFF* or *H_OFF* strains and applied
450 the Dox regimen or PBS vehicle starting at the same time of infection (0 h) or 6 h after infection
451 (Fig. S8A). For both strains, administration of Dox from the beginning of infection triggered a
452 significant improvement in survival compared with the non-treated conditions (50% VS 17.2%
453 for *51A_OFF*, *P*=0.0036, and 41.45% VS 6.67% for *H_OFF*, *P*=0.022) (Fig. 6A). Notably, the
454 administration of Dox at the time of infection, with either strain, did not improve survival to
455 close to 100%. Considering that both strains are unable to grow in the presence of the drug (Fig.
456 S6B, S7B), this was a surprising result that suggests the levels of Dox reached *in vivo* are not
457 sufficient to completely downregulate gene expression. This could be due to a rapid
458 metabolization of the drug in the larvae hemocoel or to microenvironment variations in its
459 concentration. Despite this caveat of the model, we observed that administration of Dox 6 h
460 after infection also triggered a significant improvement in survival for both strains (42.8% VS
461 17.2% for *51A_OFF*, *P*=0.0007, and 32.26% VS 6.67% for *H_OFF*, *P*=0.0324) (Fig. 6A). Therefore,
462 downregulation of methionine synthase genetic expression in established infections conferred
463 a significant benefit in survival which was comparable to that observed with the target of the
464 azoles.

465 The positive results obtained using the *Galleria* infection model prompted us to assay the
466 TetOFF system in a leukopenic murine model of pulmonary aspergillosis. To ensure that Dox
467 levels in mouse lungs reach and maintain sufficient concentrations to downregulate gene
468 expression (according to our results *in vitro*) we performed a pilot Dox dosage experiment in
469 immunosuppressed non-infected mice (Fig S8B). We extracted lungs of Dox treated mice at
470 different time-points, homogenated them and measured Dox concentration using a bioassay
471 based on inhibition of *Escherichia coli DH5α* growth. We could detect promising levels of Dox in
472 all mice (concentrations ranging from 2.2 to 0.94 µg/mL –Fig. S8B–) which according to our
473 results *in vitro* should be sufficient to downregulate gene expression from the TetOFF system.
474 We therefore infected leukopenic mice with 10^5 spores of the *51A_OFF* or the *H_OFF* strains and
475 administered PBS vehicle or our Dox regimen, starting 16 h after infection (Fig. S8B). The use of
476 an uninfected, Dox treated control group uncovered that the intense Dox regimen used was
477 harmful for the mice. These uninfected mice lost weight at a similar rate as the infected groups
478 and looked ill from the third or fourth day of treatment. This might be due to a toxic effect
479 caused by the previously described iron chelating properties of Dox (68), although we have made
480 no attempt to confirm this. As a consequence, there was no beneficial effect of Dox treatment
481 on survival (not shown). The fact that Dox treatment did also not show any benefit in survival
482 for our control strain *51A_OFF*, which should mimic treatment with azoles (primary therapy for
483 invasive aspergillosis), indicates that the TetOFF system is not ideal to mimic a drug treatment
484 in established infections. Nevertheless, we further attempted to determine the efficiency of
485 targeting MetH in established infections by measuring fungal burdens in lungs of treated and
486 untreated mice. We observed that two and a half days of Dox treatment (when there are no
487 visible toxic effects) did result in a significant reduction of fungal burdens 3 days after infection
488 for both *51A_OFF* (P=0.0279) and *H_OFF* (P=0.0019) (Fig. 6B). Therefore, we could observe a
489 beneficial effect of interfering with methionine synthase genetic expression in an established
490 pulmonary infection, which was comparable to that of interfering with the expression of *cyp51A*,
491 the target of azoles. This constitutes a very rigorous validation of MetH as a promising antifungal
492 target.

493 A recent study also aimed to use another TetOFF system to validate a drug target in
494 established aspergillosis infections (69). These authors administered Dox exclusively through
495 oral gavage, accounting for lower dosage of drug. Consequently, even if no toxic effect was
496 observed, they did also not detect any beneficial effect on survival when the Dox treatment was
497 initiated after infection. Therefore, even if the TetOFF system is currently the only model that

498 allows investigating the efficiency of new targets in aspergillosis established infections, it is
499 clearly not optimal and better models are needed.

500

501 *Structural-based virtual screening of MetH*

502 Having shown *in vivo* that MetH is a promising target, we decided to investigate its druggability
503 by running a structural-based virtual screening. The sequence of *A. fumigatus* MetH (AfMetH)
504 contains two predicted methionine synthase domains with a β-barrel fold conserved in other
505 fungal and bacterial enzymes. The structure of the *C. albicans* orthologue (70) (CaMetH) showed
506 that the active site is located between the two domains where the methyl tetrahydrofolate, the
507 homocysteine substrate and the catalytic zinc ion bind in close proximity. The homology model
508 for AfMetH (Fig. 7A) overlaps very well with that of the CaMetH thus providing a suitable
509 molecular model for further analysis. In contrast, the structure of the human methionine
510 synthase (hMS) shows a very different overall arrangement with the folate and homocysteine
511 binding domains located in completely different regions (Fig. 7B). Comparison of the
512 tetrahydrofolate binding sites between the fungal and the human structures also highlights
513 significant structural differences that affect the conformation adopted by the ligand. In the
514 CaMetH structure the 5-methyl-tetrahydrofolate (C2F) adopts a bent conformation (<20Å long)
515 and it is in close proximity to the methionine product, whereas in the human structure the
516 tetrahydrofolate (THF) ligand binds in an elongated conformation extending up to 30Å from end
517 to end, (Fig. 7 C&D).

518 Virtual screening (VS) was carried on the AfMetH and the hMS structures with the Maybridge
519 Ro3 fragment library to explore potential venues for drug development. The results showed four
520 ligand binding clusters in the AfMetH structure, two of which (C1, C2) match the binding position
521 of the 5-methyl-tetrahydrafolate and the methionine from the CaMetH crystal structure (Fig.
522 7E). For the hMS, we found two main clusters, C1 that overlaps with the tetrahydrofolate binding
523 site and C2 in a nearby pocket. Clearly the distribution of the clusters defines a very different
524 landscape around the folate site between the human and the fungal enzymes. Furthermore, the
525 proximity of the C1 and C2 clusters, matching the folate and Met/homocysteine binding sites in
526 the Ca/Af proteins means that it may be possible to combine ligands at both sites to generate
527 double-site inhibitors with high specificity towards the fungal enzymes. Antifolates are a class of
528 drugs that antagonise folate, blocking the action of folate dependent enzymes such as
529 dihydrofolate reductase (DHFR), thymidylate synthase or methionine synthase. Methotrexate is
530 an antifolate commonly used to treat cancer and autoimmune diseases. Interestingly,

531 methotrexate has been shown to be a weak inhibitor of the *C. albicans* methionine synthase
532 (32) and to have some antifungal activity against *C. albicans* (71) and *Aspergillus ssp* (72).
533 Nevertheless, methotrexate is not a good antifungal drug, as its activity is high against human
534 enzymes (IC_{50} of 0.3 µM for DHFR (73)) and low against fungal methionine synthase (IC_{50} of 4
535 mM for *C. albicans* MetH (32)). Therefore, more potent and specific inhibitors of fungal
536 methionine synthases are needed to fully exploit the value of this target for antifungal therapy,
537 a task that seems possible and can be directed from our analyses.

538

539 In summary, we have shown that methionine synthase blockage triggers not only methionine
540 auxotrophy, but also a metabolic imbalance that results in a drop in cellular energetics and
541 growth arrest. In light of our results, we stress that conditional essentiality is important to
542 understand the underlying mechanisms of metabolic processes and needs to be considered to
543 achieve proper validation of novel antimicrobial targets. Accordingly, we proved that targeting
544 methionine synthase in established infections has a beneficial effect similar to that observed for
545 the target of azoles, the most effective drugs for the treatment of aspergillosis. Finally, we
546 showed that fungal methionine synthases have distinct druggable pockets that can be exploited
547 to design specific inhibitors. In conclusion, we have demonstrated that fungal methionine
548 synthases are promising targets for the development of novel antifungals

549

550 **MATERIAL AND METHODS**

551 *Strains, media and culture conditions*

552 The *Escherichia coli* strain DH5α (74) was used for cloning procedures. Plasmid-carrying *E. coli*
553 strains were routinely grown at 37°C in LB liquid medium (Oxoid) under selective conditions (100
554 $\mu g \cdot mL^{-1}$ ampicillin or 50 $\mu g \cdot mL^{-1}$ kanamycin); for growth on plates, 1.5% agar was added to
555 solidify the medium. All plasmids used in the course of this study were generated using the
556 Seamless Cloning (Invitrogen) technology as previously described (17, 75). *E. coli* strain BL21
557 (DE3) (76) was grown on Mueller Hinton agar (Sigma) in bioassays, to determine Dox
558 concentrations within homogenized murine lungs.

559 The wild-type clinical isolate *Aspergillus fumigatus* strain ATCC 46645 served as reference
560 recipient. *A. fumigatus* strain A1160 (*ku80Δ*) (77) was also used to confirm *metH* essentiality. *A.*
561 *fumigatus* mutants were generated using a standard protoplasting protocol (78). *A. fumigatus*
562 strains were generally cultured in minimal medium (MM) (79) (1% glucose, 5 mM ammonium
563 tartrate, 7 mM KCl, 11 mM KH_2PO_4, 0.25 mM $MgSO_4$, 1× Hutner's trace elements solution; pH

564 5.5; 1.5% agar) at 37°C. For selection in the presence of resistance markers 50 µg·mL^{-1} of
565 hygromycin B or 100 µg·mL^{-1} of pyrithiamine (InvivoGen) were applied. In sulfur-free medium
566 (MM-S), $MgCl_2$ substituted for $MgSO_4$ and a modified mixture of trace elements lacking any
567 sulfate salt was used. For all growth assays on solid media, the culture medium was inoculated
568 with 10 µl of a freshly prepared *A. fumigatus* spore suspension (10^5 conidia·mL^{-1} in water
569 supplemented with 0.9% NaCl and 0.02% Tween 80) and incubated at 37°C for 3 days.

570 *Extraction and manipulation of nucleic acids*

571 Standard protocols of recombinant DNA technology were carried out (80). Phusion® high-fidelity
572 DNA polymerase (ThermoFisher Scientific) was generally used in polymerase chain reactions and
573 essential cloning steps were verified by sequencing. Fungal genomic DNA was prepared
574 following the protocol of Kolar *et al.* (81) and Southern analyses were carried out as described
575 (82, 83), using the Amersham ECL Direct Labeling and Detection System® (GE Healthcare). Fungal
576 RNA was isolated using TRIzol reagent (ThermoFisher Scientific) and Qiagen plant RNA extraction
577 kit. Retrotranscription was performed using SuperScript III First-Strand Synthesis (ThermoFisher
578 Scientific). RT-PCR on both gDNA and cDNA was performed using the SYBR® Green JumpStart
579 (Sigma) in a 7500 Fast Real Time PCR cycler from Applied Biosystems.

580 *Microscopy*

581 10^3 *A. fumigatus* resting or 8 h germinated conidia were inoculated in 200 µL of medium (+/-
582 Dox) in 8 well imaging chambers (ibidi) and incubated at 37°C. Microscopy images were taken
583 on a Nikon Eclipse TE2000-E, using a CFI Plan Apochromat Lambda 20X/0.75 objective and
584 captured with a Hamamatsu Orca-ER CCD camera (Hamamatsu Photonics) and manipulated
585 using NIS-Elements 4.0 (Nikon). For extensively grown mycelia a stereomicroscope Leica MZFL-
586 III was used, with a Q-imaging Retinga 6000 camera, and manipulated using Metamorph v7760.
587 Confocal imaging was performed using a Leica TCS SP8x inverted confocal microscope equipped
588 with a 40X/0.85 objective. Nuclei were stained with DAPI (Life Technologies Ltd) as described
589 previously (84). GFP was excited at 458 nm with an Argon laser at 20% power. DAPI was excited
590 at 405 nm with an LED diode at 20%.

591 *Metabolome analyses*

592 *A. fumigatus* wild-type and *metH_tetOFF* strains were incubated in MM for 16 h before the -Dox
593 samples were taken (8 replicates of 11 mL each). Then, 5 µg/mL Dox and 5 mM methionine (to
594 prevent metabolic adaptation due to met auxotrophy) were added as appropriate and the
595 cultures incubated for 6 h, after which the +Dox samples were taken (8 × 11 mL). The samples
596 were immediately quenched with 2× volumes of 60% methanol at -48°C. After centrifugation at

597 4800 *g* for 10 min at -8°C, metabolites were extracted in 1 mL 80% methanol at -48°C by three
598 cycles of N_2 liquid snap freezing, thawing and vortexing. Supernatant was cleared by
599 centrifugation at -9 °C, 14,500 *g* for 5 min. Quality control (QC) samples were prepared by
600 combining 100 µL from each sample. Samples were aliquoted (300 µL), followed by the addition
601 of 100 µL of the internal standard solution (0.2 mg/mL succinic-d_4 acid, and 0.2 mg/mL glycine-
602 *d*5) and vortex mix for 15 s. All samples were lyophilised by speed vacuum concentration at room
603 temperature overnight (HETO VR MAXI vacuum centrifuge attached to a Thermo Svart RVT 4104
604 refrigerated vapour trap; Thermo Life Sciences, Basingstoke, U.K.). A two-step derivatization
605 protocol of methoxyamination followed by trimethylsilylation was employed (85).

606 GC-MS analysis was conducted on a 7890B GC coupled to a 5975 series MSD quadrupole
607 mass spectrometer and equipped with a 7693 autosampler (Agilent, Technologies, UK). The
608 sample (1 µL) was injected onto a VF5-MS column (30 m x 0.25 mm x 0.25 µm; Agilent
609 Technologies) with an inlet temperature of 280 °C and a split ratio of 20:1. Helium was used as
610 the carrier gas with a flow rate of 1 mL/min. The chromatography was programmed to begin at
611 70 °C with a hold time of 4 min, followed by an increase to 300 °C at a rate of 14 °C/min and a
612 final hold time of 4 min before returning to 70 °C. The total run time for the analysis was 24.43
613 min. The MS was equipped with an electron impact ion source using 70 eV ionisation and a fixed
614 emission of 35 µA. The mass spectrum was collected for the range 50-550 m/z with a scan speed
615 of 3,125 (*N*=1). Samples were analysed in a randomised order with the injection of a pooled
616 biological quality control sample after every 6th sample injection.

617 For data analysis, the GC-MS raw files were converted to mzXML and subsequently imported
618 to R. The R package "erah" was employed to de-convolve the GC-MS files. Chromatographic
619 peaks and mass spectra were cross-referenced with the Golm library for putative identification
620 purposes, and followed the metabolomics standards initiative (MSI) guidelines for metabolite
621 identification (86). The peak intensities were normalised according to the IS (succinic-d_4 acid)
622 before being $\log_{10}$-scaled for further statistical analysis. All pre-processed data were investigated
623 by employing principal component analysis (PCA) (87).

624 The raw data of this metabolome analysis has been deposited in the MetaboLights database
625 (88), under the reference MTBLS1636 (www.ebi.ac.uk/metabolights/MTBLS1636)

626 *ATP Quantitation*

627 *A. fumigatus* was grown as in the metabolome analysis. However, where the effect of SAM was
628 investigated spores were inoculated into MM-N + 1mg/mL aac and 0.5mM SAM was also added
629 at the time of Dox addition. ATP levels were determined using the BacTiter-Glo™ Assay

630 (Promega) following the manufacturer's instructions and a TriStar LB 941 Microplate Reader
631 (Berthold).

632 *Isolation and detection of SAM*

633 *A. fumigatus* was grown exactly in the same conditions as described for the metabolome
634 analysis. Harvested mycelia were snap-frozen in liquid N_2 and stored at -70 °C before SAM
635 isolation. SAM extraction was carried out according to Owens *et al* (89). Briefly, frozen mycelia
636 were ground in liquid N_2 and 0.1 M HCl (250 µL) was added to ground mycelia (100 mg). Samples
637 were stored on ice for 1 h, with sample vortexing at regular intervals. Samples were centrifuged
638 at 13,000 *g* for 10 min (4 °C) to remove cell debris and supernatants were collected.
639 Concentration of protein in supernatants was determined using a Biorad Bradford protein assay
640 relative to a bovine serum albumin (BSA) standard curve. Clarified supernatants were adjusted
641 to 15 % (w/v) trichloroacetic acid to remove protein. After 20 min incubation on ice,
642 centrifugation was repeated and clarified supernatants were diluted with 0.1 % (v/v) formic acid.
643 Samples were injected onto a Hypersil Gold aQ C18 column with polar endcapping on a Dionex
644 UltiMate 3000 nanoRSLC with a Thermo Q-Exactive mass spectrometer. Samples were loaded in
645 100 % Solvent A (0.1 % (v/v) formic acid in water) followed by a gradient to 20 % B (Solvent B:
646 0.1 % (v/v) formic acid in acetonitrile) over 4 min. Resolution set to 70000 for MS, with MS/MS
647 scans collected using a Top3 method. SAM standard (Sigma) was used to determine retention
648 time and to confirm MS/MS fragmentation pattern for identification. Extracted ion
649 chromatograms were generated at m/z 399-400 and the peak area of SAM was measured.
650 Measurements were taken from three biological and two technical replicates per sample,
651 normalized to the protein concentration in the extracts from each replicate. SAM levels are
652 expressed as a percentage relative to the parental strain in the absence of Dox.

653 *Nuclei isolation and Western Blot*

654 Protoplasts were generated as in *A. fumigatus* transformations and nuclei isolated were isolated
655 by sucrose gradient fractionation as previously described by Sperling and Grunstein (90). Nuclear
656 localisation of GFP-tagged target proteins was confirmed by Western-blot. Aliquots of nuclei
657 were boiled for 5 minutes in loading buffer (0.2 M Tris-HCl, 0.4 M DTT, 8% SDS, trace
658 bromophenol blue) and separated on a 12% (w/v) SDS-PAGE gel. The proteins were transferred
659 to a Polyvinylidene difluoride (PVDF) membrane using the Trans-Blot® Turbo™ Transfer System
660 (Bio-Rad). Detection of GFP was carried out with a rabbit polyclonal anti-GFP antiserum (Bio-
661 Rad) and anti-rabbit IgG HRP-linked antibody (Cell Signalling Technology). SuperSignal West Pico
662 PLUS Chemiluminescent Substrate (Thermo Scientific) and the ChemiDoc XRS+ Imaging System

663 (Biorad) were used to visualise immunoreactive bands. Ponceau S staining was performed to
664 normalize the Western-blot signal to the protein loading.

665 *Biomass measurement*

666 Conidia were inoculated into MM-S, supplemented with either methionine or sulfate, and
667 incubated at 37°C 180 rpm for 12, 16 or 24 h. After this initial incubation, 3 mL samples were
668 taken in triplicate from the cultures, filtered through tared Miracloth, dried at 60°C for 16 h and
669 their biomass measured. In treated conditions Dox was added to a final concentration of 1
670 µg/mL and the culture allowed to grow for a further 24 h at 37°C 180 rpm. 5 mL samples were
671 taken in triplicate and their biomass measured as above.

672 *Galleria mellonella infections*

673 Sixth-stage instar larval *G. mellonella* moths (15 to 25 mm in length) were ordered from the Live
674 Foods Company (Sheffield, United Kingdom). Infections were performed according to Kavanagh
675 and Fallon (91). Randomly selected groups of 15 larvae were injected in the last left proleg with
676 10 µL of a suspension of 5×10^4 conidia/mL in PBS, using Braun Omnican 50-U 100 0.5- mL insulin
677 syringes with integrated needles. Dox was administered according to the treatment shown in
678 Fig. S8A, alternating injections in the last right and left prolegs. In each experiment an untouched
679 and a saline injected control were included, to verify that mortality was not due to the health
680 status of the larvae or the injection method. Three independent experiments were carried out.
681 The presented survival curves display the pooled data, which was analysed with the Log-Rank
682 test.

683 *Ethics Statement*

684 All mouse experiments were performed under United Kingdom Home Office project license
685 PDF8402B7 and approved by the University of Manchester Ethics Committee and by the
686 Biological Services Facility at the Faculty of Biology, Medicine and Health, University of
687 Manchester.

688 *Leukopenic murine model of invasive pulmonary aspergillosis and calculation of fungal burden.*

689 Outbred CD1 male mice (22– 26 g) were purchased from Charles Rivers and left to rest for at
690 least 1 week before the experiment. Mice were allowed access *ad libitum* to water and food
691 throughout the experiment. Mice were immunosuppressed with 150 mg/kg of
692 cyclophosphamide on days -3 and -1 and with 250 mg/kg cortisone acetate on day -1. On day 0
693 mice were anesthetized with isofluorane and intranasally infected with a dose of 10^5 conidia (40
694 µL of a freshly harvested spore solution of 2.5×10^6 conidia/mL). Dox was administered
695 according to the treatment shown in Fig. S8B. Dox containing food was purchased from Envingo

696 (Safe-diet U8200 Version 0115 A03 0.625 g/kg Doxycycline Hyclate pellets). At the selected time-
697 point (72 h after infection for fungal burden) mice were sacrificed by a lethal injection of
698 pentobarbital, the lungs harvested and immediately frozen.

699 Frozen lungs were lyophilised for 48 h in a CoolSafe ScanVac freeze drier connected to a
700 VacuuBrand pump and subsequently ground in the presence of liquid nitrogen. DNA was
701 isolated from the powder using the DNeasy Blood & Tissue Kit (Qiagen). DNA concentration and
702 quality were measured using a NanoDrop 2000 (ThermoFisher Scientific). To detect the fungal
703 burden, 500 ng of DNA extracted from each infected lung were subjected to qPCR. Primers used
704 to amplify the *A. fumigatus* β-tubulin gene (AFUA_7G00250) were forward, 5'-
705 ACTTCCGCAATGGACGTTAC-3', and reverse, 5'- GGATGTTGTTGGGAATCCAC-3'. Those designed
706 to amplify the murine actin locus (NM_007393) were forward, 5'-CGAGCACAGCTTCTTTGCAG-3'
707 and reverse, 5'-CCCATGGTGTCCGTTCTGA-3'. Standard curves were calculated using different
708 concentrations of fungal and murine gDNA pure template. Negative controls containing no
709 template DNA were subjected to the same procedure to exclude or detect any possible
710 contamination. Three technical replicates were prepared for each lung sample. qPCRs were
711 performed using the 7500 Fast Real-Time PCR system (Thermo Fisher Scientific) with the
712 following thermal cycling parameters: 94 °C for 2 min and 40 cycles of 94°C for 15 s and 59°C for
713 1 min. The fungal burden was calculated by normalising the number of fungal genome
714 equivalents (i.e. number of copies of the tubulin gene) to the murine genome equivalents in the
715 sample (i.e number of copies of the actin gene) (92). Two independent experiments were
716 carried out (*n*=9, 5 mice in the first and 4 mice in the second experiment). Burdens for each
717 strain were compared using a Mann Whitney test.

718 *Molecular homology models and virtual screening*

719 The full-length sequence for AFUA_4G07360, the cobalamin-independent methionine synthase
720 MetH from *A. fumigatus* (AfMetH) was obtained from FungiDB (https://fungidb.org/fungidb)
721 (93). This sequence together with the structure of the *C. albicans* orthologue (CaMetH) (PDB ID:
722 4L65, DOI: 10.1016/j.jmb.2014.02.006) were used to create the molecular homology model in
723 Modeller (version 9.23) (94) with the basic option mode. The AfMetH model was then used for
724 virtual screening with the semi-automated pipeline VSpipe (95). For comparison we also
725 performed virtual screening with the structure of the human methionine synthase (hMS)
726 containing the folate and homocysteine binding domains (PDB ID: 4CCZ). Docking was done
727 using the Maybridge Ro3 1000 fragment library with AutoDock Vina (96). Results were inspected
728 graphically using PyMol (v1.8.0.3 Enhanced for Mac OS X (Schrödinger). All images were
729 produced with PyMol.

730 **ACKNOWLDGEMENTS**

731 We acknowledge the use of the Phenotyping Center at Manchester (PCAM) for the use of their
732 microscopes and advanced image analysis workstations. We are grateful to Prof Sven
733 Krappmann for critical reading of the manuscript and his constant support. We would like to
734 thank all members of MFIG for constant help and encouragement.

735 JA was supported by a MRC Career Development Award (MR/N008707/1). JS was supported by
736 a BSAC scholarship (bsac-2016-0049). BPT was supported by a MRC Doctoral Training
737 Partnership PhD studentship. Q-Exactive mass spectrometer and nanoLC instrumentation were
738 funded by a competitive infrastructure award from Science Foundation Ireland (SFI)
739 (12/RI/2346(3)).

740

741 **AUTHOR CONTRIBUTION**

742 JS performed the majority of experiments, analysed and interpreted most of the data and
743 participated in the design of the project. MS helped with the acquisition and analysis of most of
744 the experiments. BT run the structural-based virtual screening. RAO measured SAM levels in
745 mycelia. HMA performed the metabolomic experiment, analysed and with RG interpreted the
746 data. RFG assisted with the mouse models of infection. RT helped with the execution of qPCRs.
747 KH helped to set up the GC-MS instrument. SD designed the MS/MS analysis of SAM. RG
748 designed the metabolome analysis and interpreted the data. LT designed the virtual screening
749 analysis and interpreted the data. EB participated in the design and conception of the project.
750 JA conceived and designed the project and analysed most of the data.

751

752 **COMPETING INTERESTS**

753 The authors declare no competing interests.

754 **DATA AVAILABILITY**

755 The raw data that support the findings of this study are available upon reasonable request to
756 the authors. The raw data of metabolome analysis has been deposited in the MetaboLights
757 database [85], under the reference MTBLS1636 (www.ebi.ac.uk/metabolights/MTBLS1636).

758

759

760 **REFERENCES**

761 1. Fisher MC, Hawkins NJ, Sanglard D, Gurr SJ. Worldwide emergence of resistance to
762 antifungal drugs challenges human health and food security. Science. 2018;360(6390):739-
763 42.
764 2. Bongomin F, Gago S, Oladele RO, Denning DW. Global and Multi-National Prevalence of
765 Fungal Diseases-Estimate Precision. J Fungi (Basel). 2017;3(4).
766 3. Bitar D, Lortholary O, Le Strat Y, Nicolau J, Coignard B, Tattevin P, et al. Population-based
767 analysis of invasive fungal infections, France, 2001-2010. Emerg Infect Dis. 2014;20(7):1149-
768 55.
769 4. Brown GD, Denning DW, Gow NA, Levitz SM, Netea MG, White TC. Hidden killers: human
770 fungal infections. Sci Transl Med. 2012;4(165):165rv13.
771 5. Nyazika TK, Hagen F, Machiridza T, Kutepa M, Masanganise F, Hendrickx M, et al.
772 *Cryptococcus neoformans* population diversity and clinical outcomes of HIV-associated
773 cryptococcal meningitis patients in Zimbabwe. J Med Microbiol. 2016;65(11):1281-8.
774 6. Patterson TF, Thompson GR, 3rd, Denning DW, Fishman JA, Hadley S, Herbrecht R, et al.
775 Executive Summary: Practice Guidelines for the Diagnosis and Management of Aspergillosis:
776 2016 Update by the Infectious Diseases Society of America. Clin Infect Dis. 2016;63(4):433-
777 42.
778 7. Pound MW, Townsend ML, Dimondi V, Wilson D, Drew RH. Overview of treatment options
779 for invasive fungal infections. Med Mycol. 2011;49(6):561-80.
780 8. Ghannoum MA, Rice LB. Antifungal agents: mode of action, mechanisms of resistance, and
781 correlation of these mechanisms with bacterial resistance. Clin Microbiol Rev.
782 1999;12(4):501-17.
783 9. Verweij PE, Chowdhary A, Melchers WJ, Meis JF. Azole Resistance in *Aspergillus fumigatus*:
784 Can We Retain the Clinical Use of Mold-Active Antifungal Azoles? Clin Infect Dis.
785 2016;62(3):362-8.
786 10. Amich J, Krappmann S. Deciphering metabolic traits of the fungal pathogen *Aspergillus*
787 *fumigatus*: redundancy vs. essentiality. Frontiers in Microbiology. 2012;Fungi and Their
788 Interactions(In Press.).
789 11. Kaltdorf M, Srivastava M, Gupta SK, Liang C, Binder J, Dietl AM, et al. Systematic
790 Identification of Anti-Fungal Drug Targets by a Metabolic Network Approach. Front Mol
791 Biosci. 2016;3:22.
792 12. Oliver JD, Sibley GEM, Beckmann N, Dobb KS, Slater MJ, McEntee L, et al. F901318
793 represents a novel class of antifungal drug that inhibits dihydroorotate dehydrogenase.
794 Proc Natl Acad Sci U S A. 2016;113(45):12809-14.
795 13. Evans JC, Huddler DP, Hilgers MT, Romanchuk G, Matthews RG, Ludwig ML. Structures of
796 the N-terminal modules imply large domain motions during catalysis by methionine
797 synthase. Proceedings of the National Academy of Sciences of the United States of America.
798 2004;101(11):3729-36.
799 14. Peariso K, Zhou ZHS, Smith AE, Matthews RG, Penner-Hahn JE. Characterization of the zinc
800 sites in cobalamin-independent and cobalamin-dependent methionine synthase using zinc
801 and selenium X-ray absorption spectroscopy. Biochemistry. 2001;40(4):987-93.
802 15. Gonzalez JC, Banerjee RV, Huang S, Sumner JS, Matthews RG. Comparison of cobalamin-
803 independent and cobalamin-dependent methionine synthases from *Escherichia coli:* two
804 solutions to the same chemical problem. Biochemistry. 1992;31(26):6045-56.
805 16. Matthews RG, Smith AE, Zhou ZHS, Taurog RE, Bandarian V, Evans JC, et al. Cobalamin-
806 dependent and cobalamin-independent methionine synthases: Are there two solutions to
807 the same chemical problem? Helvetica Chimica Acta. 2003;86(12):3939-54.
808 17. Amich J, Dumig M, O'Keeffe G, Binder J, Doyle S, Beilhack A, et al. Exploration of Sulfur
809 Assimilation of *Aspergillus fumigatus* Reveals Biosynthesis of Sulfur-Containing Amino Acids
810 as a Virulence Determinant. Infect Immun. 2016;84(4):917-29.

811 18.Segal ES, Gritsenko V, Levitan A, Yadav B, Dror N, Steenwyk JL, et al. Gene Essentiality
812 Analyzed by In Vivo Transposon Mutagenesis and Machine Learning in a Stable Haploid
813 Isolate of *Candida albicans*. MBio. 2018;9(5).
814 19.Suliman HS, Appling DR, Robertus JD. The gene for cobalamin-independent methionine
815 synthase is essential in *Candida albicans*: a potential antifungal target. Arch Biochem
816 Biophys. 2007;467(2):218-26.
817 20.Pascon RC, Ganous TM, Kingsbury JM, Cox GM, McCusker JH. *Cryptococcus neoformans*
818 methionine synthase: expression analysis and requirement for virulence. Microbiology.
819 2004;150(Pt 9):3013-23.
820 21.Li W, Cowley A, Uludag M, Gur T, McWilliam H, Squizzato S, et al. The EMBL-EBI
821 bioinformatics web and programmatic tools framework. Nucleic Acids Res.
822 2015;43(W1):W580-4.
823 22.McWilliam H, Li W, Uludag M, Squizzato S, Park YM, Buso N, et al. Analysis Tool Web
824 Services from the EMBL-EBI. Nucleic Acids Res. 2013;41(Web Server issue):W597-600.
825 23.Miwa GT. The Drug Discovery Process In: Lu C, Li AP, editors. Enzyme Inhibition in Drug
826 Discovery and Development: The Good and the Bad:

827 Wiley Online Library 2010. p. 1-14.
828 24.Cook D, Brown D, Alexander R, March R, Morgan P, Satterthwaite G, et al. Lessons learned
829 from the fate of AstraZeneca's drug pipeline: a five-dimensional framework. Nature
830 Reviews Drug Discovery. 2014;13(6):419-31.
831 25.Wanka F, Cairns T, Boecker S, Berens C, Happel A, Zheng X, et al. Tet-on, or Tet-off, that is
832 the question: Advanced conditional gene expression in *Aspergillus*. Fungal Genet Biol.
833 2016;89:72-83.
834 26.Scott J, Sueiro-Olivares M, Ahmed W, Heddergott C, Zhao C, Thomas R, et al. *Pseudomonas*
835 *aeruginosa*-Derived Volatile Sulfur Compounds Promote Distal *Aspergillus fumigatus*
836 Growth and a Synergistic Pathogen-Pathogen Interaction That Increases Pathogenicity in
837 Co-infection. Front Microbiol. 2019;10:2311.
838 27.Lucock M. Folic acid: nutritional biochemistry, molecular biology, and role in disease
839 processes. Mol Genet Metab. 2000;71(1-2):121-38.
840 28.Tzin V, Galili G. The Biosynthetic Pathways for Shikimate and Aromatic Amino Acids in
841 *Arabidopsis thaliana*. Arabidopsis Book. 2010;8:e0132.
842 29.Deakova Z, Durackova Z, Armstrong DW, Lehotay J. Two-dimensional high performance
843 liquid chromatography for determination of homocysteine, methionine and cysteine
844 enantiomers in human serum. J Chromatogr A. 2015;1408:118-24.
845 30.Elshorbagy AK, Jerneren F, Samocha-Bonet D, Refsum H, Heilbronn LK. Serum S-
846 adenosylmethionine, but not methionine, increases in response to overfeeding in humans.
847 Nutr Diabetes. 2016;6:e192.
848 31.Jochim A, Shi T, Belikova D, Schwarz S, Peschel A, Heilbronner S. Methionine Limitation
849 Impairs Pathogen Expansion and Biofilm Formation Capacity. Appl Environ Microbiol.
850 2019;85(9).
851 32.Ubhi D, Kago G, Monzingo AF, Robertus JD. Structural analysis of a fungal methionine
852 synthase with substrates and inhibitors. J Mol Biol. 2014;426(8):1839-47.
853 33.Sahu U, Rajendra VKH, Kapnoor SS, Bhagavat R, Chandra N, Rangarajan PN. Methionine
854 synthase is localized to the nucleus in *Pichia pastoris* and *Candida albicans* and to the
855 cytoplasm in *Saccharomyces cerevisiae*. J Biol Chem. 2017;292(36):14730-46.
856 34.Fujita Y, Ukena E, Iefuji H, Giga-Hama Y, Takegawa K. Homocysteine accumulation causes a
857 defect in purine biosynthesis: further characterization of *Schizosaccharomyces pombe*
858 methionine auxotrophs. Microbiology. 2006;152(Pt 2):397-404.
859 35.Gems D, Johnstone IL, Clutterbuck AJ. An autonomously replicating plasmid transforms
860 *Aspergillus nidulans* at high frequency. Gene. 1991;98(1):61-7.

861 36.Aleksenko AY, Clutterbuck AJ. Recombinational stability of replicating plasmids in
862 *Aspergillus nidulans* during transformation, vegetative growth and sexual reproduction.
863 Curr Genet. 1995;28(1):87-93.
864 37.Paul S, Klutts JS, Moye-Rowley WS. Analysis of promoter function in *Aspergillus fumigatus*.
865 Eukaryot Cell. 2012;11(9):1167-77.
866 38.Christopher SA, Melnyk S, James SJ, Kruger WD. S-adenosylhomocysteine, but not
867 homocysteine, is toxic to yeast lacking cystathionine beta-synthase. Mol Genet Metab.
868 2002;75(4):335-43.
869 39.Perna AF, Ingrosso D, Lombardi C, Acanfora F, Satta E, Cesare CM, et al. Possible
870 mechanisms of homocysteine toxicity. Kidney Int Suppl. 2003(84):S137-40.
871 40.Bretes E, Zimny J. Homocysteine thiolactone affects protein ubiquitination in yeast. Acta
872 Biochim Pol. 2013;60(3):485-8.
873 41.Jakubowski H. Pathophysiological consequences of homocysteine excess. J Nutr.
874 2006;136(6 Suppl):1741S-9S.
875 42.Lopez-Ibanez J, Pazos F, Chagoyen M. MBROLE 2.0-functional enrichment of chemical
876 compounds. Nucleic Acids Research. 2016;44(W1):W201-W4.
877 43.Chong J, Soufan O, Li C, Caraus I, Li SZ, Bourque G, et al. MetaboAnalyst 4.0: towards more
878 transparent and integrative metabolomics analysis. Nucleic Acids Research.
879 2018;46(W1):W486-W94.
880 44.Xia JG, Psychogios N, Young N, Wishart DS. MetaboAnalyst: a web server for metabolomic
881 data analysis and interpretation. Nucleic Acids Research. 2009;37:W652-W60.
882 45.Fendt SM, Sauer U. Transcriptional regulation of respiration in yeast metabolizing
883 differently repressive carbon substrates. BMC Syst Biol. 2010;4:12.
884 46.Akita O, Nishimori C, Shimamoto T, Fujii T, Iefuji H. Transport of pyruvate in *Saccharomyces*
885 *cerevisiae* and cloning of the gene encoded pyruvate permease. Biosci Biotechnol Biochem.
886 2000;64(5):980-4.
887 47.Forte GM, Davie E, Lie S, Franz-Wachtel M, Ovens AJ, Wang T, et al. Import of extracellular
888 ATP in yeast and man modulates AMPK and TORC1 signalling. J Cell Sci. 2019;132(7).
889 48.Hu W, Sillaots S, Lemieux S, Davison J, Kauffman S, Breton A, et al. Essential gene
890 identification and drug target prioritization in *Aspergillus fumigatus*. PLoS Pathog.
891 2007;3(3):e24.
892 49.Beattie SR, Mark KMK, Thammahong A, Ries LNA, Dhingra S, Caffrey-Carr AK, et al.
893 Filamentous fungal carbon catabolite repression supports metabolic plasticity and stress
894 responses essential for disease progression. PLoS Pathog. 2017;13(4):e1006340.
895 50.Cramer RA. *In vivo* veritas: *Aspergillus fumigatus* proliferation and pathogenesis--
896 conditionally speaking. Virulence. 2016;7(1):7-10.
897 51.Kowalski CH, Kerkaert JD, Liu KW, Bond MC, Hartmann R, Nadell CD, et al. Fungal biofilm
898 morphology impacts hypoxia fitness and disease progression. Nat Microbiol.
899 2019;4(12):2430-41.
900 52.Gorman MW, Feigl EO, Buffington CW. Human plasma ATP concentration. Clin Chem.
901 2007;53(2):318-25.
902 53.Ito S, Furuya K, Sokabe M, Hasegawa Y. Cellular ATP release in the lung and airway. Aims
903 Biophysics. 2016;3(4):571-84.
904 54.Mortaz E, Braber S, Nazary M, Givi ME, Nijkamp FP, Folkerts G. ATP in the pathogenesis of
905 lung emphysema. Eur J Pharmacol. 2009;619(1-3):92-6.
906 55.Riteau N, Gasse P, Fauconnier L, Gombault A, Couegnat M, Fick L, et al. Extracellular ATP Is
907 a Danger Signal Activating P2X(7) Receptor in Lung Inflammation and Fibrosis. American
908 Journal of Respiratory and Critical Care Medicine. 2010;182(6):774-83.
909 56.Walvekar AS, Srinivasan R, Gupta R, Laxman S. Methionine coordinates a hierarchically
910 organized anabolic program enabling proliferation. Mol Biol Cell. 2018;29(26):3183-200.
911 57.De Virgilio C, Loewith R. The TOR signalling network from yeast to man. Int J Biochem Cell
912 Biol. 2006;38(9):1476-81.

913 58.Loewith R, Hall MN. Target of rapamycin (TOR) in nutrient signaling and growth control.
914 Genetics. 2011;189(4):1177-201.
915 59.Saxton RA, Sabatini DM. mTOR Signaling in Growth, Metabolism, and Disease. Cell.
916 2017;168(6):960-76.
917 60.Thiepold AL, Lorenz NI, Foltyn M, Engel AL, Dive I, Urban H, et al. Mammalian target of
918 rapamycin complex 1 activation sensitizes human glioma cells to hypoxia-induced cell
919 death. Brain. 2017;140(10):2623-38.
920 61.Tsouko E, Khan AS, White MA, Han JJ, Shi Y, Merchant FA, et al. Regulation of the pentose
921 phosphate pathway by an androgen receptor-mTOR-mediated mechanism and its role in
922 prostate cancer cell growth. Oncogenesis. 2014;3:e103.
923 62.Baldin C, Valiante V, Kruger T, Schafferer L, Haas H, Kniemeyer O, et al. Comparative
924 proteomics of a tor inducible *Aspergillus fumigatus* mutant reveals involvement of the Tor
925 kinase in iron regulation. Proteomics. 2015;15(13):2230-43.
926 63.Caza M, Kronstad JW. The cAMP/Protein Kinase a Pathway Regulates Virulence and
927 Adaptation to Host Conditions in *Cryptococcus neoformans*. Front Cell Infect Microbiol.
928 2019;9:212.
929 64.Grosse C, Heinekamp T, Kniemeyer O, Gehrke A, Brakhage AA. Protein kinase A regulates
930 growth, sporulation, and pigment formation in *Aspergillus fumigatus*. Appl Environ
931 Microbiol. 2008;74(15):4923-33.
932 65.Gerke J, Bayram O, Braus GH. Fungal S-adenosylmethionine synthetase and the control of
933 development and secondary metabolism in *Aspergillus nidulans*. Fungal Genet Biol.
934 2012;49(6):443-54.
935 66.Bauer I, Misslinger M, Shadkchan Y, Dietl AM, Petzer V, Orasch T, et al. The Lysine
936 Deacetylase RpdA Is Essential for Virulence in *Aspergillus fumigatus*. Front Microbiol.
937 2019;10:2773.
938 67.Stewart JIP, Fava VM, Kerkaert JD, Subramanian AS, Gravelat FN, Lehoux M, et al. Reducing
939 *Aspergillus fumigatus* Virulence through Targeted Dysregulation of the Conidiation
940 Pathway. mBio. 2020;11(1).
941 68.Grenier D, Huot MP, Mayrand D. Iron-chelating activity of tetracyclines and its impact on
942 the susceptibility of *Actinobacillus actinomycetemcomitans* to these antibiotics. Antimicrob
943 Agents Chemother. 2000;44(3):763-6.
944 69.Peng Y, Zhang H, Xu M, Tan MW. A Tet-Off gene expression system for validation of
945 antifungal drug targets in a murine invasive pulmonary aspergillosis model. Sci Rep.
946 2018;8(1):443.
947 70.Ferrer JL, Ravanel S, Robert M, Dumas R. Crystal structures of cobalamin-independent
948 methionine synthase complexed with zinc, homocysteine, and methyltetrahydrofolate. J
949 Biol Chem. 2004;279(43):44235-8.
950 71.Warnock DW, Johnson EM, Burke J, Pracharktam R. Effect of methotrexate alone and in
951 combination with antifungal drugs on the growth of *Candida albicans*. J Antimicrob
952 Chemother. 1989;23(6):837-47.
953 72.Yang J, Gao L, Yu P, Kosgey JC, Jia L, Fang Y, et al. In vitro synergy of azole antifungals and
954 methotrexate against *Candida albicans*. Life Sci. 2019;235:116827.
955 73.Fan CC, Vitols KS, Huennekens FM. Inhibition of dihydrofolate reductase by methotrexate: a
956 new look at an old problem. Adv Enzyme Regul. 1980;18:41-52.
957 74.Woodcock DM, Crowther PJ, Doherty J, Jefferson S, DeCruz E, Noyer-Weidner M, et al.
958 Quantitative evaluation of *Escherichia coli* host strains for tolerance to cytosine methylation
959 in plasmid and phage recombinants. Nucleic Acids Res. 1989;17(9):3469-78.
960 75.Amich J, Schafferer L, Haas H, Krappmann S. Regulation of sulphur assimilation is essential
961 for virulence and affects iron homeostasis of the human-pathogenic mould *Aspergillus*
962 *fumigatus*. PLoS Pathog. 2013;9(8):e1003573.
963 76.Wood WB. Host specificity of DNA produced by *Escherichia coli*: bacterial mutations
964 affecting the restriction and modification of DNA. J Mol Biol. 1966;16(1):118-33.

965 77.da Silva Ferreira ME, Kress MR, Savoldi M, Goldman MH, Hartl A, Heinekamp T, et al. The
966 akuB(KU80) mutant deficient for nonhomologous end joining is a powerful tool for
967 analyzing pathogenicity in *Aspergillus fumigatus*. Eukaryot Cell. 2006;5(1):207-11.
968 78.Szewczyk E, Nayak T, Oakley CE, Edgerton H, Xiong Y, Taheri-Talesh N, et al. Fusion PCR and
969 gene targeting in *Aspergillus nidulans*. Nat Protoc. 2006;1(6):3111-20.
970 79.Kafer E. Meiotic and mitotic recombination in *Aspergillus* and its chromosomal aberrations.
971 Adv Genet. 1977;19:33-131.
972 80.Sambrook J, Fritsch EF, Maniatis T. Molecular Cloning: A Laboratory Manual. Press CSHL,
973 editor. NY.1989.
974 81.Kolar M, Punt PJ, van den Hondel CA, Schwab H. Transformation of *Penicillium*
975 *chrysogenum* using dominant selection markers and expression of an *Escherichia coli lacZ*
976 fusion gene. Gene. 1988;62(1):127-34.
977 82.Southern E. Southern blotting. Nat Protoc. 2006;1(2):518-25.
978 83.Southern EM. Detection of specific sequences among DNA fragments separated by gel
979 electrophoresis. J Mol Biol. 1975;98(3):503-17.
980 84.Reverberi M, Punelli M, Smith CA, Zjalic S, Scarpari M, Scala V, et al. How peroxisomes
981 affect aflatoxin biosynthesis in *Aspergillus flavus*. PLoS One. 2012;7(10):e48097.
982 85.Wedge DC, Allwood JW, Dunn W, Vaughan AA, Simpson K, Brown M, et al. Is Serum or
983 Plasma More Appropriate for Intersubject Comparisons in Metabolomic Studies? An
984 Assessment in Patients with Small-Cell Lung Cancer. Analytical Chemistry.
985 2011;83(17):6689-97.
986 86.Sumner LW, Amberg A, Barrett D, Beale MH, Beger R, Daykin CA, et al. Proposed minimum
987 reporting standards for chemical analysis. Metabolomics. 2007;3(3):211-21.
988 87.Gromski PS, Muhamadali H, Ellis DI, Xu Y, Correa E, Turner ML, et al. A tutorial review:
989 Metabolomics and partial least squares-discriminant analysis - a marriage of convenience or
990 a shotgun wedding. Analytica Chimica Acta. 2015;879:10-23.
991 88.Haug K, Cochrane K, Nainala VC, Williams M, Chang J, Jayaseelan KV, et al. MetaboLights: a
992 resource evolving in response to the needs of its scientific community. Nucleic Acids Res.
993 2020;48(D1):D440-D4.
994 89.Owens RA, O'Keeffe G, Smith EB, Dolan SK, Hammel S, Sheridan KJ, et al. Interplay between
995 Gliotoxin Resistance, Secretion, and the Methyl/Methionine Cycle in *Aspergillus fumigatus*.
996 Eukaryot Cell. 2015;14(9):941-57.
997 90.Sperling AS, Grunstein M. Histone H3 N-terminus regulates higher order structure of yeast
998 heterochromatin. Proc Natl Acad Sci U S A. 2009;106(32):13153-9.
999 91.Kavanagh K, Fallon JP. *Galleria mellonella* larvae as models for studying fungal virulence.
1000 Fungal Biol Rev. 2010;24:79-83.
1001 92.Gago S, Buitrago MJ, Clemons KV, Cuenca-Estrella M, Mirels LF, Stevens DA. Development
1002 and validation of a quantitative real-time PCR assay for the early diagnosis of
1003 coccidioidomycosis. Diagn Microbiol Infect Dis. 2014;79(2):214-21.
1004 93.Stajich JE, Harris T, Brunk BP, Brestelli J, Fischer S, Harb OS, et al. FungiDB: an integrated
1005 functional genomics database for fungi. Nucleic Acids Res. 2012;40(Database issue):D675-
1006 81.
1007 94.Fiser A, Sali A. MODELLER: Generation and refinement of homology-based protein structure
1008 models. Macromolecular Crystallography, Pt D. 2003;374:461-91.
1009 95.Alvarez-Carretero S, Pavlopoulou N, Adams J, Gilsenan J, Tabernero L. VSpipe, an Integrated
1010 Resource for Virtual Screening and Hit Selection: Applications to Protein Tyrosine
1011 Phospahatase Inhibition. Molecules. 2018;23(2).
1012 96.Trott O, Olson AJ. Software News and Update AutoDock Vina: Improving the Speed and
1013 Accuracy of Docking with a New Scoring Function, Efficient Optimization, and
1014 Multithreading. Journal of Computational Chemistry. 2010;31(2):455-61.

1015

1016

1017 **Figure 1. Methionine synthase (MetH) enzymatic activity is essential for *A. fumigatus* viability.**

1018 **A)** Schematic representation of the trans-sulfuration pathway and its intersection with the one
1019 carbon metabolic route. **B)** Both strains, a *ΔmetF* mutant (which blocks the one carbon
1020 metabolism route) and a *ΔmetGΔcysD* mutant (which blocks the trans-sulfuration pathway)
1021 could grow in the presence of methionine. In contrast, the *metH_tetOFF* strain (*H_OFF*) could
1022 not grow in restrictive conditions (+Dox) even if methionine was supplemented. The phenotypic
1023 analysis was repeated in three independent experiments. Representative plates are shown. **C)**
1024 A second copy of the *metH* gene under the control of its own promoter was introduced in the
1025 innocuous *Ku70* locus of the *H_OFF* background strain. Two point-mutated versions of the gene
1026 were introduced, one that causes a D→A substitution in amino acid 616 and another one that
1027 causes a Y→A substitution in amino acid 662. In non-restrictive conditions all strains were able
1028 to grow as the parental *H_OFF* strain. In the presence of Dox and absence of met, the Y662A
1029 protein was able to trigger significant growth, suggesting that its enzymatic activity is impaired
1030 but not blocked. In the presence of Met the Y662A strain grew as well in restrictive as in non-
1031 restrictive conditions, suggesting that partial enzymatic activity is sufficient to cover the
1032 essential function of MetH. In restrictive conditions and absence of methionine, the D616A
1033 strain was not able to grow, indicating that enzymatic activity is blocked in this mutated protein.
1034 The D616A was also not able to grow in the presence of Dox and met, indicating that enzymatic
1035 activity is required for the essential function of MetH. The phenotypic analysis was repeated in
1036 three independent experiments. Representative plates are shown.

1037

1038 **Figure 2. Shortage of important downstream metabolites, but not toxic accumulation of**
1039 **homocysteine, partially accounts for MetH essentiality.**

1040 **A)** Supplementation of the growth media with a variety of downstream metabolites (Fig. 1A)
1041 showed that purines (adenine A and guanine G, 3 mM) could slightly reconstitute growth of the
1042 *H_OFF* strain in restrictive conditions. Further supplementation of amino acids improves growth,
1043 but not to the wild-type levels. Folic acid (5 mM) could also reconstitute growth when amino
1044 acids are the only N-source. **B)** Overexpression of genes that could detoxify a potential
1045 accumulation of homocysteine did not reconstitute growth in the absence of MetH activity.
1046 Further addition of adenine did not improve growth. The phenotypic analyses were repeated in
1047 three independent experiments. Representative plates are shown.

1048

1049 **Figure 3. Lack of methionine synthase activity causes a decrease in cell energetics.**

1050 **A)** Normalized concentrations of metabolites in fungal mycelia (*n*=8). Adenosine levels were
1051 decreased in *H_OFF*+Dox compared with *wt*+Dox, which agrees with its capacity to partially
1052 reconstitute growth. Several metabolites of the glycolysis and TCA pathways were reduced in
1053 *H_OFF*+Dox compared with *wt*+Dox, suggesting low energetic levels. **B)** The levels of ATP
1054 significantly decreased in the *H_OFF* strain upon Dox addition, whilst they did not vary
1055 significantly in the *wt* strain. Each point represents a biological replicate, which was assayed with
1056 three technical replicates. Data was analysed using one sample *t*-test to a hypothetical value of
1057 100 (i.e. no change in ratio of ATP). Graph displays the mean and standard deviation. **C)** Pyruvate
1058 as the sole carbon source could reconstitute growth of the *H_OFF* strain in restrictive conditions
1059 to wild-type levels. For both strains, growth was limited and slightly improved in the presence
1060 of amino acids. ATP could fully reconstitute growth of *H_OFF* when amino acids were the sole
1061 N-source. The phenotypic analyses were repeated in three independent experiments.
1062 Representative plates are shown. **D)** RT-PCR calculation of the fold-change in genetic expression

1063 of *metF* and *G6PD* with respect to their expression in wild-type without Dox. Each point
1064 represents a biological replicate which was analysed with three technical replicates. Data was
1065 analysed using one sample *t*-test to a hypothetical value of 1 (i.e. no change in expression).
1066 Graphs display the mean and standard deviation. **E)** Schematic representation of the metabolic
1067 imbalance started with MetH repression (1). Lack of the enzymatic activity caused a shortage of
1068 5,10-methylene-THF and consequently of purine rings (2). This was sensed as a shortage of
1069 nucleotides that the cell attempted to compensate through an unknown mechanism, seemingly
1070 TOR and PKA independent (3), that activated glucose flow through the Pentose Phosphate
1071 Pathway (PPP) (4). That caused a reduction of glycolysis and TCA cycles, which in turn decreased
1072 ATP levels (5). ATP usage for *S*-adenosylmethionine (SAM) synthesis was maintained, which
1073 caused a drop in cell energy that resulted in growth arrest (6). Genes/pathways/compounds
1074 expected to be reduced are highlighted in green and those increased in magenta.

1075

1076 **Figure 4. External *S*-adenosylmethionine (SAM) reconstitutes ATP levels and growth.**

1077 **A)** Addition of SAM to the medium reconstituted growth of the *H_OFF* strain in restrictive
1078 conditions. The phenotypic analysis was repeated in two independent experiments.
1079 Representative plates are shown. **B)** Levels of SAM did not significantly decrease upon Dox
1080 administration (5 µg/mL) in wild-type or *H_OFF* strains. Graphs depict mean and SD of three
1081 biological and two technical replicates. Data were analysed using one-way ANOVA with
1082 Bonferroni post-tests adjustment. **C)** Presence of SAM in the medium (0.5 mM) prevented the
1083 decrease in ATP levels observed in the *H_OFF* strain upon Dox addition. In fact, ATP levels were
1084 increased compared to the minus Dox condition. Graphs depict mean and SD of two biological
1085 and four technical replicates. **D)** Expression of MetH-GFP in the *H_OFF* background showed that
1086 the protein localised both in cytoplasm and nucleus.

1087

1088 **Figure 5. Repression of *metH* transcription causes inhibition of growth *in vitro.***

1089 **A)** Addition of 1 µg/mL Dox to 12 and 16 h grown mycelia strongly reduced fungal biomass,
1090 measured 24 h later. This was more pronounced in media without methionine. The effect was
1091 lost when Dox was added 24 h after inoculation. For comparison, fungal biomass of mycelia
1092 harvested at the time of Dox addition (12, 16 and 24 h post-inoculation) is shown. Three
1093 independent experiments were performed, using 3 technical replicates for each. **B)** Microscopic
1094 images of 8 h germinated spores treated with 10 µg/mL Dox. Images were taken 16 h after Dox
1095 addition (wide-field microscopy) and again 24 h later (stereomicroscopy). Dox addition halts
1096 growth of *H_OFF* strain in a sustained manner. **C)** Time-lapse microscopy of *H_OFF* growth upon
1097 Dox addition. Dox was added to 8 h grown conidia, which caused growth inhibition that was
1098 obvious after ~4 h. Growth was virtually halted for as long as Dox was present. **D)** ~6 h after Dox
1099 withdrawal, *H_OFF* growth resumed, showing that the effect was fungistatic.

1100

1101 **Figure 6. Downregulation of *metH in vivo* in established infections shows a beneficial effect**
1102 **comparable to the target of azoles.**

1103 **A)** Administration of a Dox regimen (Fig. S8A) to *Galleria mellonella* infected with either the
1104 *H_OFF* strain or the *51A_OFF* control strain showed a beneficial effect in survival. For both
1105 strains, starting regimen at the time of infection triggered a significant improvement in survival
1106 (50% VS 17.2% for *51A_OFF*, *P*=0.0036, and 41.45% VS 6.67% for *H_OFF*, *P*=0.022). Dox regimen
1107 6 h after infection also triggered a significant improvement in survival for both strains (42.8% VS
1108 17.2% for *51A_OFF*, *P*=0.0007, and 32.26% VS 6.67% for *H_OFF*, *P*=0.0324). The curves show the
1109 pooled data from 3 independent experiments. Curves were compared using the Log-Rank test.

1110 **B)** Leukopenic mice were infected with *51A_OFF* or *H_OFF* and a Dox regimen (Fig. S8B)
1111 administered 16 h after infection. Upon Dox treatment, fungal burden in the lungs was
1112 significantly reduced for both strains (*P*=0.0279 for *51A_OFF* and *P*=0.0019 for *H_OFF*). Two
1113 independent experiment were carried out. Each point in the graphs represents one mouse (n=9).
1114 Burdens for each strain were compared using a Mann Whitney test.

1115

1116 **Figure 7. Virtual-screening of fungal and human methionine synthases reveals different**
1117 **druggability of the proteins.**

1118 **A)** The structures of the crystallized *C. albicans* and the predicted A. *fumigatus* methionine
1119 synthases are highly similar. **B)** In contrast, the structure of the human enzyme is very different,
1120 having he 5-methyl-tetrahydrafolate and homocysteine binding sites separated. **C)** Detail of the
1121 active site of fungal methionine synthases, with the methionine, folate and zinc displayed. **D)**
1122 Tetrahydrofolate binding site of the human protein. **E)** Virtual screening on the *A. fumigatus*
1123 protein found four ligand binding clusters in the structure, two of which (C1, C2) match the
1124 binding position of the 5-methyl-tetrahydrafolate and the methionine. **F)** In the human enzyme
1125 two clusters were found, one (C1) that overlaps with the tetrahydrofolate binding site and
1126 (another C2) in a nearby pocket.

1127

1128

1129

1130

1131

1132

1133

1134

1135

1136

1137

1138

1139

1140

1141

1142

1143

1144 **SUPPLEMENTARY FIGURES**

1145 **Figure S1.**

1146 **A)** Addition of 1 µg/mL Dox to a 16 h growing mycelia quickly downregulated transcription of
1147 *metH*. **B)** The growth of two *metH_tetOFF* strains in two different backgrounds was prevented
1148 in the presence of as little as 0.5 µg/mL Dox, even in the presence of methionine. The phenotypic
1149 analysis was repeated in three independent experiments. Representative plates are shown. **C)**
1150 An *A. fumigatus ΔmetGΔcysD* mutant (methionine auxotroph) was completely avirulent in a
1151 leukopenic murine model of invasive pulmonary aspergillosis.

1152 **Figure S2.**

1153 **A)** Schematic representation of the pJA49 plasmid for episomal overexpression of genes in *A.*
1154 *fumigatus*. It carries the *A. nidulans* AMA1 autologous replicating sequence and the hygromycin
1155 B resistance gene (*hygrB*) as a selection marker. A unique *Stu*I restriction site allows introduction
1156 of any PCR amplified ORF in frame under the control of the *A. fumigatus* strong promoter *hspA*
1157 and the *A. nidulans trpC* terminator. **B)** Schematic representation of the genes overexpressed
1158 (in green) to eliminate potential accumulation of toxic homocysteine and derivatives (in red). **C)**
1159 Fold change in expression level of *mecA* and *sahL* measured by RT-PCR. Both genes are highly
1160 overexpressed from plasmid pJA49. **D)** Expression level of *blhA* determined by retrotranscription
1161 and PCR (fold change cannot be calculated as this gene is not expressed in *A. fumigatus*).

1162 **Figure S3.**

1163 Relevance of the nitrogen source for the capacity of different metabolites to reconstitute growth
1164 of the *H_OFF* strain in restrictive conditions. Amino acids alone were not able to reconstitute
1165 growth. Folic acid could partially, and ATP and SAM completely reconstituted growth when
1166 amino acids were the only N-source, suggesting that they are only taken up when there is a high
1167 variety of permeases in the cell membrane. Pyruvate could reconstitute growth to wild-type
1168 level in the absence of glucose and independently of the in presence of amino acids, although
1169 growth improved when they were added.

1170 **Figure S4.**

1171 **A)** Principal component analysis (PCA) scores plot of the GC-MS metabolome analysis. The wild-
1172 type and *H_OFF* strains clusters were close before addition of Dox and became clearly separated
1173 upon 6 h incubation in the presence of Dox. **B)** The content of several amino acids and sugars
1174 were reduced in the H_OFF+Dox sample compared with the developmentally matched wt+Dox
1175 sample. **C)** Neither low concentrations of rapamycin (to partially inhibit TOR) nor of H89 (to

1176 partially inhibit PKA) were able to reconstitute growth of the *H_OFF* strain in restrictive
1177 conditions. This suggests that these regulatory pathways are not responsible for the deleterious
1178 switch in metabolism that causes a drop in cellular ATP.

1179 **Figure S5.**

1180 **A)** Expression of MetH-GFP wild type and MetH^{R742A}-GFP reconstituted growth of the *H_OFF*
1181 strain in restrictive conditions, demonstrating that the proteins are active. As expected, the
1182 inactive protein MetH^{D616A}-GFP did not trigger growth. **B)** Western-blot of MetH. Strains
1183 expressing MetH-GFP wild type and MetH^{R742A}-GFP were grown in the presence of Dox, nuclei
1184 isolated from the mycelia (as described in material and methods), proteins purified and blotted
1185 with an anti-GFP antibody. The MetH^{R742A}-GFP protein could be detected in nuclei, at similar
1186 levels as the wild-type MetH-GFP.

1187 **Figure S6.**

1188 **A)** Measurement of fungal growth by Optical Density (OD) showed that addition of 1 µg/mL Dox
1189 12 or 16 h after inoculation significantly reduced fugal growth at 24 and 36 h post-incubation.
1190 **B)** Microscopy analysis of the effect of the addition of 2 concentrations of Dox to resting or 8 h
1191 germinated conidia of the *H_OFF* strain. In the absence of methionine growth is immediately
1192 halted in a sustained manner. In the presence of methionine conidia can germinate and
1193 germlings elongate the growing tube before growth stops. However, once arrested, growth is
1194 halted in a sustained manner. Microimages were taken with a wide-field microscope at 16 h
1195 post-inoculation and with a stereomicroscope 40 h after inoculation (to be able to capture the
1196 huge mass of fungal growth in the control conditions).

1197 **Figure S7.**

1198 **A)** Colony formation of the strain *cyp51A_tetOFFΔcyp51B* (*51A_OFF*) is completely prevented
1199 with as little as 0.1 µg/mL on an agar plate. Phenotypic analysis was repeated in two
1200 independent experiments. **B)** Microscopy analysis of the effect of the addition of 2
1201 concentrations of Dox to resting or 8 h germinated conidia of the 51A_*OFF* strain. In both cases
1202 growth is immediately blocked. We could observe bursting germlings with high doses of Dox
1203 (red arrow).

1204 **Figure S8.**

1205 **A)** Dox regime applied to *Galleria mellonella*. A maximum of 5 doses were applied, commencing
1206 either at the time of infection or 6 h later. **B)** Dox regimen administered to mice. Treatment
1207 started 16 h after infection with a subcutaneous (SC) Dox injection and change to Dox food.

1208 Treatment was maintained with SC injections every 12 h after the infection time-point. Dox
1209 concentration in the lungs was measured in a preliminary experiment with uninfected mice.
1210 Lungs were harvested 4 h after the beginning of treatment, 2 h after the third injection (on day
1211 2) and 9 h after the 5th (on day 3, last injection). The concentrations were determined to range
1212 from 0.9 to 2.2 µg/mL, sufficient to downregulate gene expression according to the results *in*
1213 *vitro*.

1214

1215

1216 **Video S1**

1217 Time-lapse of growth of *H_OFF* and *51A_OFF* strains upon Dox addition and withdrawal.

1218

1219

1220

Fig. 1

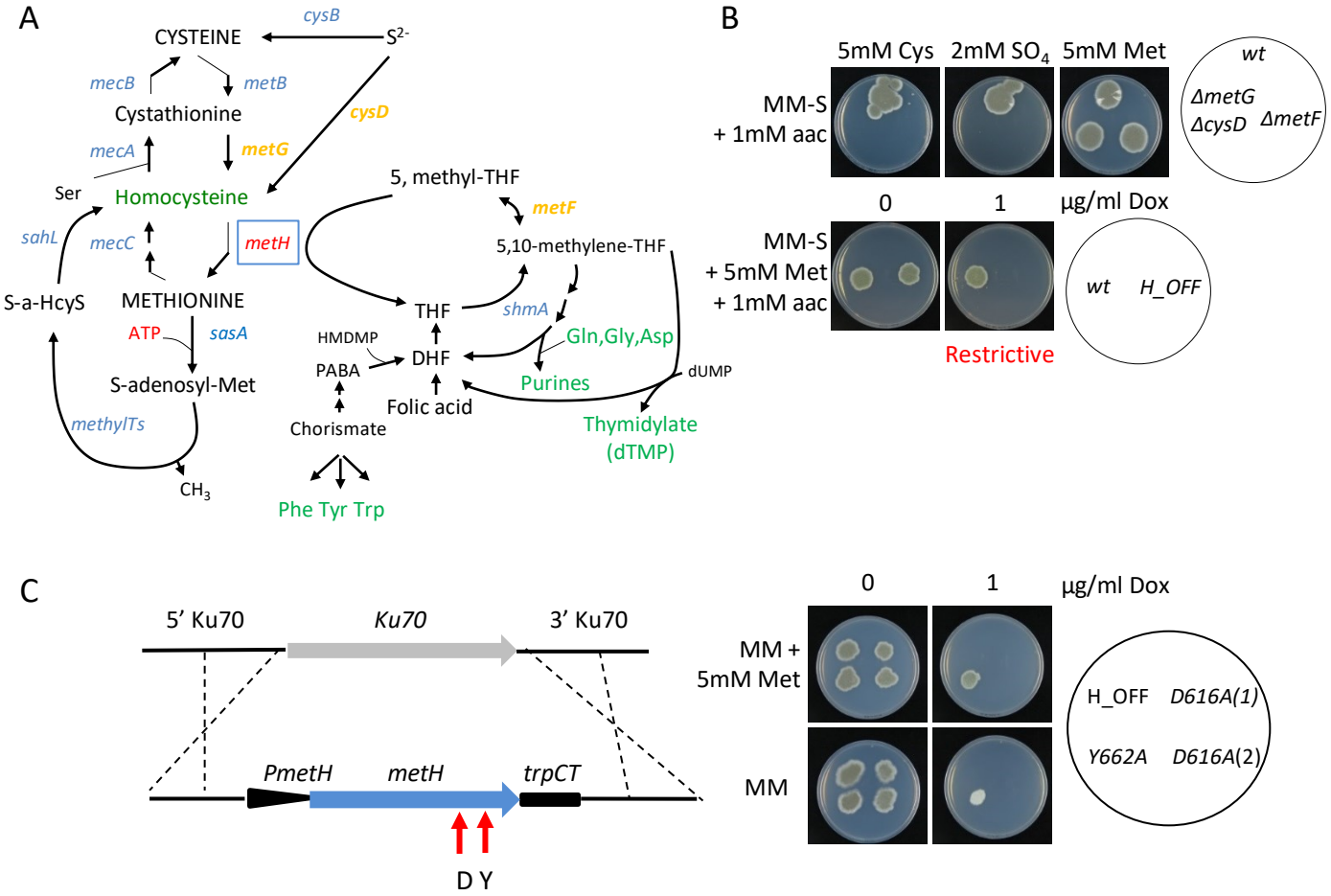
A
CYSTEINE
cysB
S2-
mecB
metB
Cystathionine
cysD
mecA
metG
Ser
Homocysteine
5, methyl-THF
metF
sahL
mecC
metH
5,10-methylene-THF
S-a-HcyS
METHIONINE
THF
shmA
ATP
sasA
HMDMP
Gln,Gly,Asp
PABA
DHF
S-adenosyl-Met
Purines
dUMP
Folic acid
methylTs
Chorismate
Thymidylate
(dTMP)
CH3
Phe Tyr Trp
B
5mM Cys
2mM SO4
5mM Met
MM-S
+ 1mM aac
wt
ΔmetG
ΔcysD
ΔmetF
0
1
µg/ml Dox
MM-S
+ 5mM Met
+ 1mM aac
wt
H_OFF
Restrictive
C
5' Ku70
Ku70
3' Ku70
PmetH
metH
trpCT
D Y
0
1
µg/ml Dox
MM +
5mM Met
MM
H_OFF
D616A(1)
Y662A
D616A(2)

Fig. 2

A

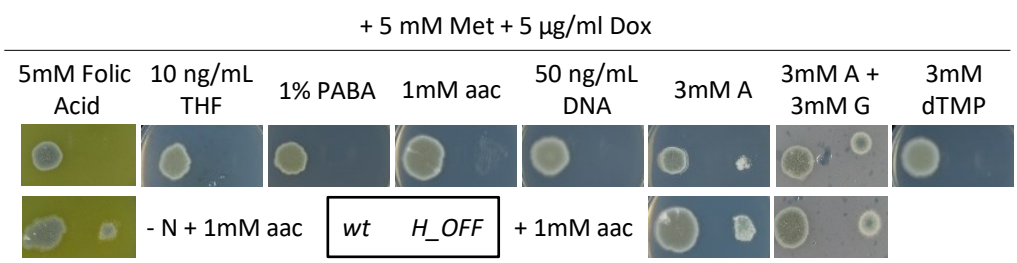
+ 5 mM Met + 5 µg/ml Dox
5mM Folic Acid
10 ng/mL THF
1% PABA
1mM aac
50 ng/mL DNA
3mM A
3mM A + 3mM G
3mM dTMP
- N + 1mM aac
wt
H_OFF
+ 1mM aac

B

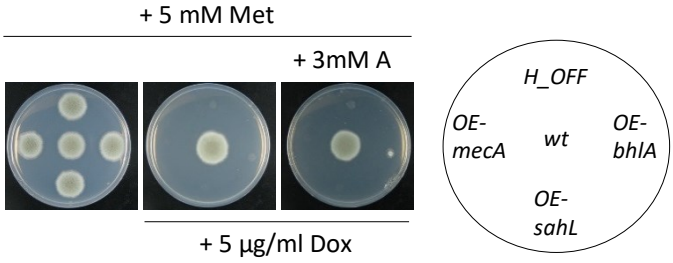
+ 5 mM Met
+ 3mM A
+ 5 µg/ml Dox
H_OFF
OE-mecA
wt
OE-bhlA
OE-sahL

Fig. 3

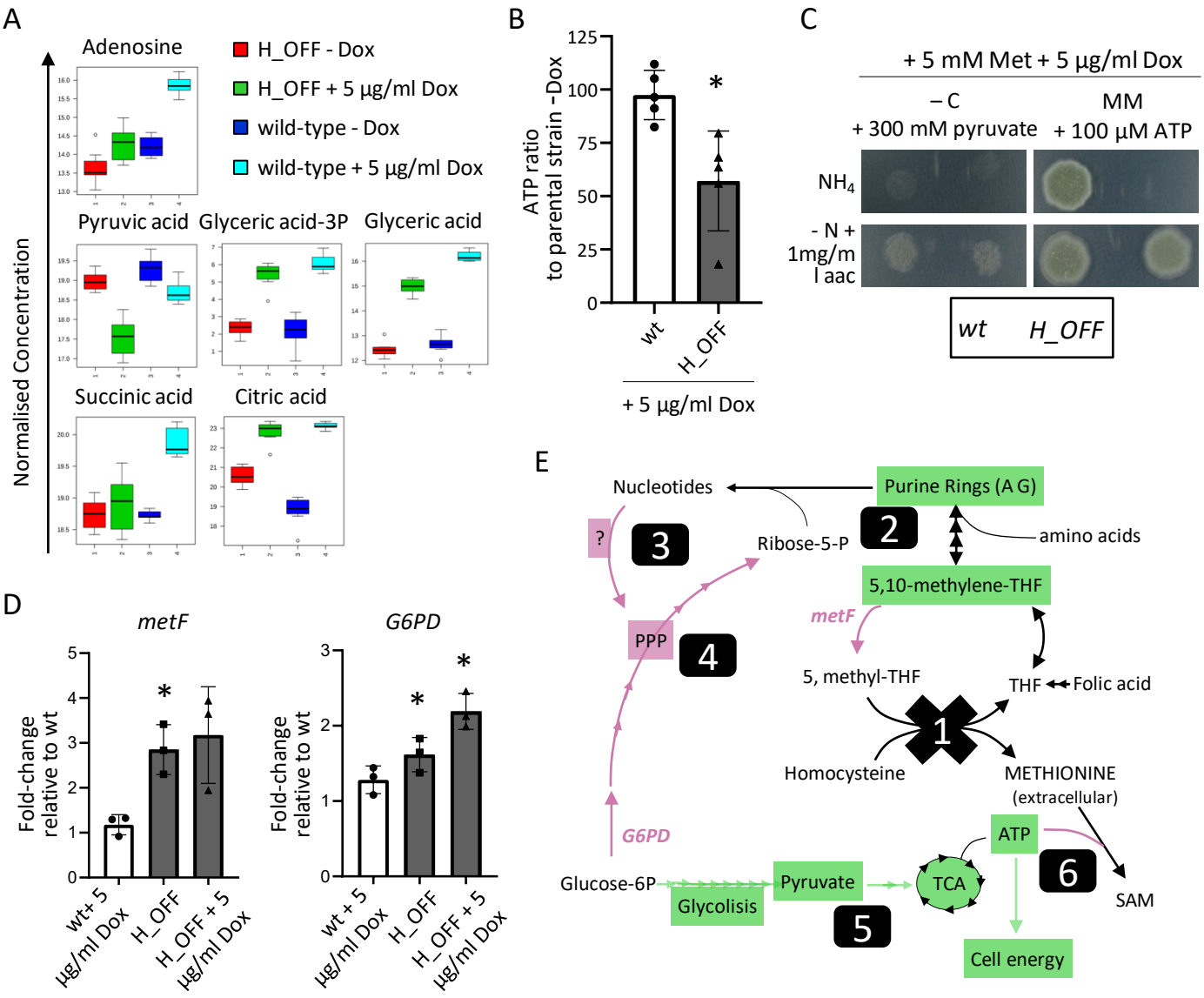
A
Adenosine
H_OFF - Dox
H_OFF + 5 µg/ml Dox
wild-type - Dox
wild-type + 5 µg/ml Dox
Pyruvic acid
Glyceric acid-3P
Glyceric acid
Succinic acid
Citric acid
Normalised Concentration
B
ATP ratio to parental strain -Dox
125
100
75
50
25
0
*
wt
H_OFF
+ 5 µg/ml Dox
C
+ 5 mM Met + 5 µg/ml Dox
– C
+ 300 mM pyruvate
MM
+ 100 µM ATP
NH4
- N + 1mg/ml aac
wt
H_OFF
D
metF
G6PD
Fold-change relative to wt
wt+ 5 µg/ml Dox
H_OFF
H_OFF + 5 µg/ml Dox
E
Nucleotides
Purine Rings (A G)
Ribose-5-P
amino acids
5,10-methylene-THF
metF
PPP
5, methyl-THF
THF
Folic acid
Homocysteine
METHIONINE (extracellular)
ATP
SAM
G6PD
Glucose-6P
Glycolisis
Pyruvate
TCA
Cell energy
?
1
2
3
4
5
6

Fig. 4

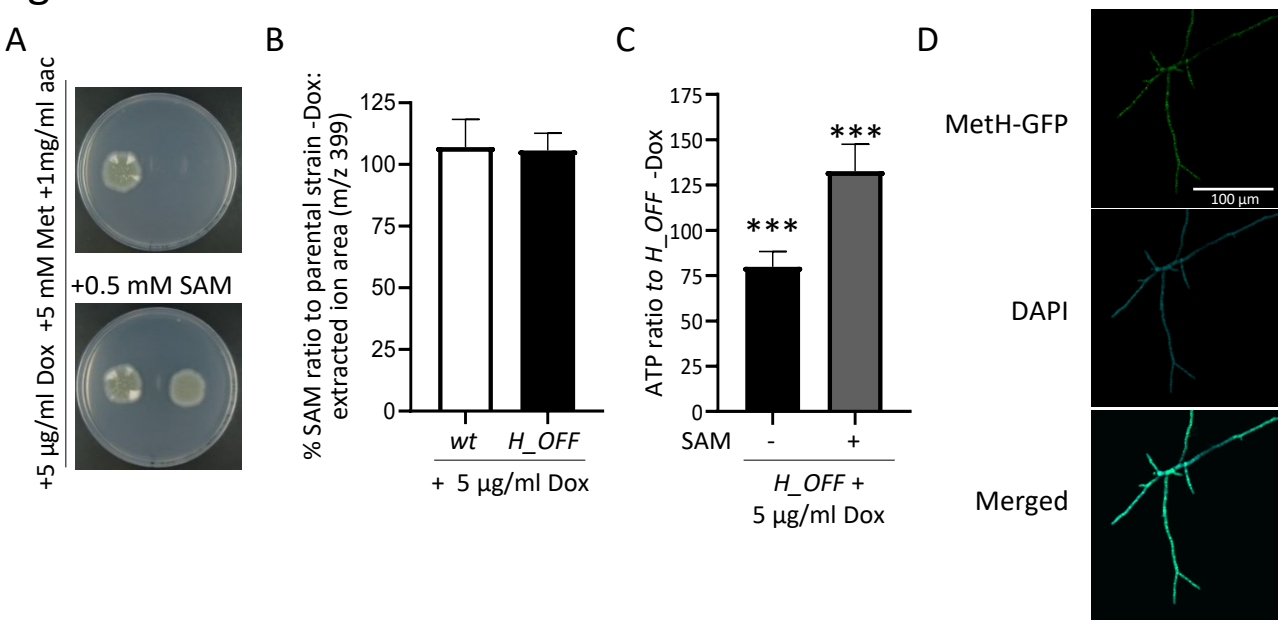
A
+5 µg/ml Dox +5 mM Met +1mg/ml aac
+0.5 mM SAM
B
% SAM ratio to parental strain -Dox: extracted ion area (m/z 399)
125
100
75
50
25
0
wt
H_OFF
+ 5 µg/ml Dox
C
ATP ratio to H_OFF -Dox
175
150
125
100
75
50
25
0
***
***
SAM
-
+
H_OFF +
5 µg/ml Dox
D
MetH-GFP
DAPI
Merged
100 µm

Fig. 5

A

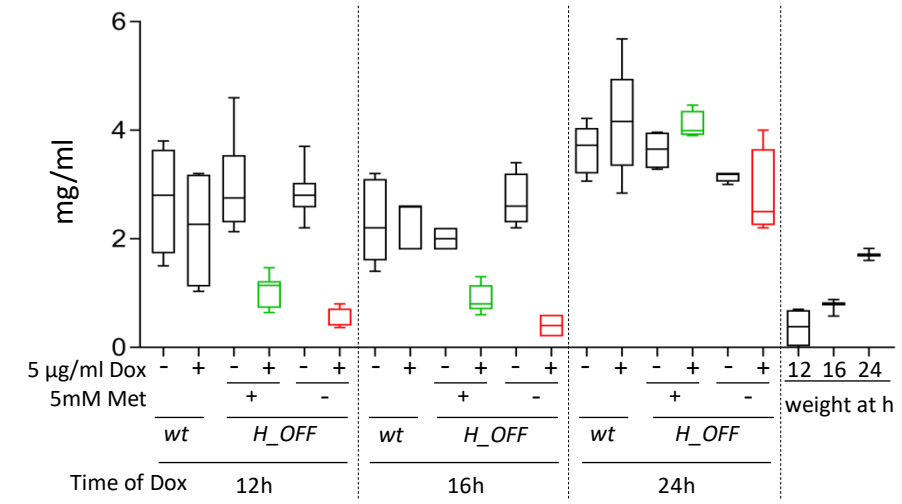
mg/ml
6
4
2
0
5 µg/ml Dox
5mM Met
wt
H_OFF
Time of Dox
12h
16h
24h
12 16 24
weight at h

B

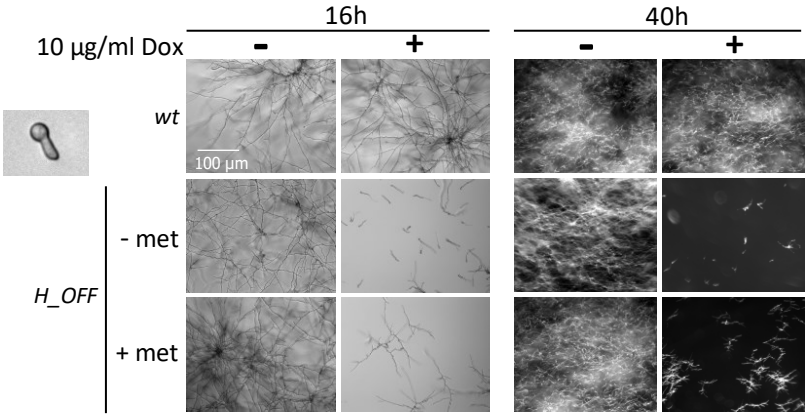
16h
40h
10 µg/ml Dox
-
+
wt
100 µm
H_OFF
- met
+ met

C

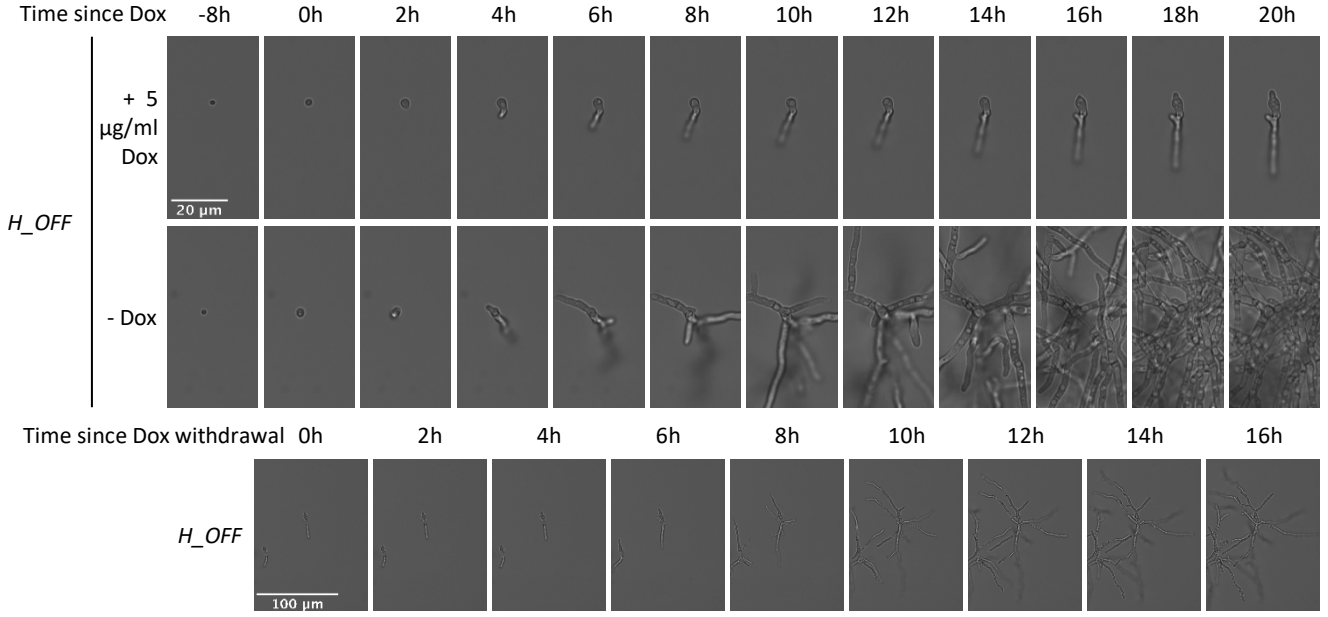
Time since Dox
-8h
0h
2h
4h
6h
8h
10h
12h
14h
16h
18h
20h
+ 5 µg/ml Dox
H_OFF
20 µm
- Dox
Time since Dox withdrawal
0h
2h
4h
6h
8h
10h
12h
14h
16h
H_OFF
100 µm

Fig. 6

A

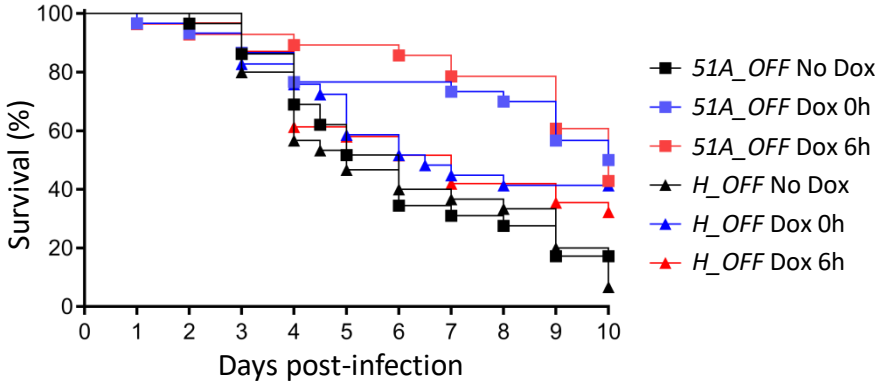
100
80
60
40
20
0
Survival (%)
0
1
2
3
4
5
6
7
8
9
10
Days post-infection
51A_OFF No Dox
51A_OFF Dox 0h
51A_OFF Dox 6h
H_OFF No Dox
H_OFF Dox 0h
H_OFF Dox 6h

B

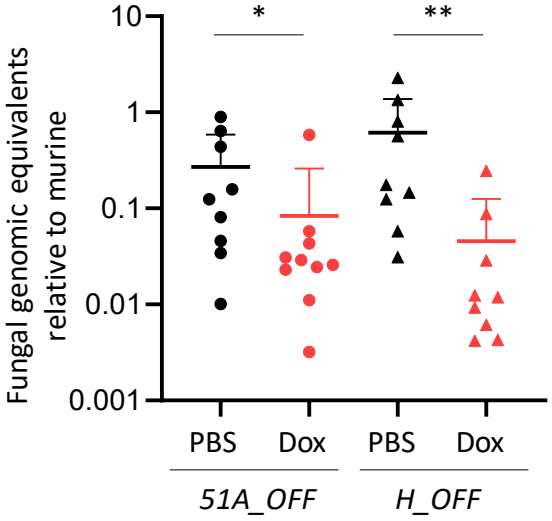
10
1
0.1
0.01
0.001
Fungal genomic equivalents relative to murine
*
**
PBS
Dox
PBS
Dox
51A_OFF
H_OFF

Fig. 7

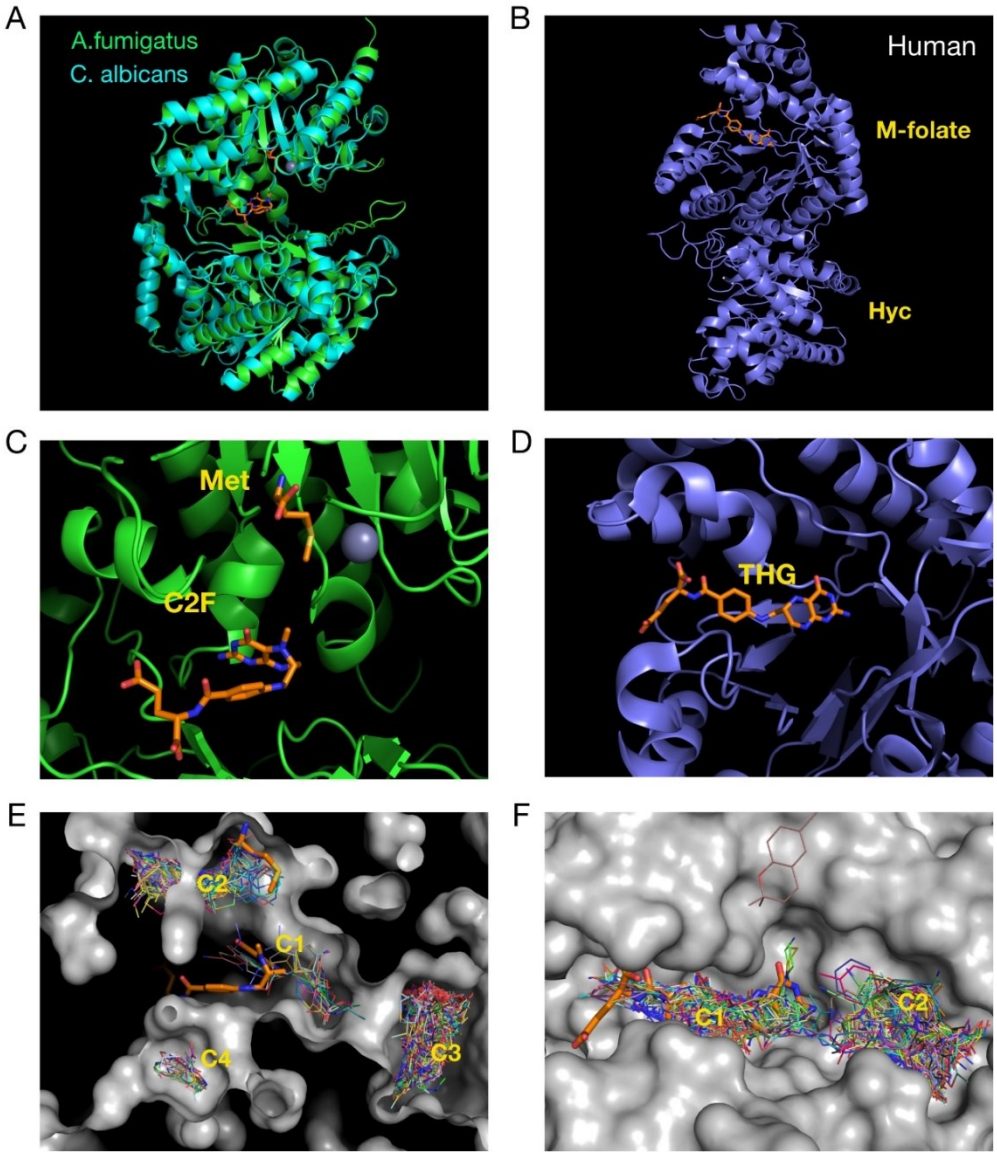
A
A.fumigatus
C. albicans
B
Human
M-folate
Hyc
C
Met
C2F
D
THG
E
C2
C1
C4
C3
F
C1
C2